

# Active Brownian motion with speed fluctuations in arbitrary dimensions: exact calculation of moments and dynamical crossovers

**Amir Shee**

Institute of Physics, Sachivalaya Marg, Bhubaneswar 751005, India  
Homi Bhaba National Institute, Anushaktigar, Mumbai 400094, India  
E-mail: [amir@iopb.res.in](mailto:amir@iopb.res.in)

**Debasish Chaudhuri**

Institute of Physics, Sachivalaya Marg, Bhubaneswar 751005, India  
Homi Bhaba National Institute, Anushaktigar, Mumbai 400094, India  
E-mail: [debc@iopb.res.in](mailto:debc@iopb.res.in)

**Abstract.** We consider the motion of an active Brownian particle with speed fluctuations in  $d$ -dimensions in the presence of both translational and orientational diffusion. We use an Ornstein-Uhlenbeck process for active speed generation. Using a Laplace transform approach, we describe and use a Fokker-Planck equation-based method to evaluate the exact time dependence of all relevant dynamical moments. We present explicit calculations of such moments and compare our analytical predictions against numerical simulations to demonstrate and analyze several dynamical crossovers. The kurtosis of displacement shows positive or negative deviations from a Gaussian behavior at intermediate times depending on the dominance of speed or orientational fluctuations.

## Contents

<b>1</b>	<b>Introduction</b>	<b>3</b>
<b>2</b>	<b>Model</b>	<b>4</b>
<b>3</b>	<b>Calculation of moments from Fokker-Planck equation</b>	<b>5</b>
<b>4</b>	<b>Active speed</b>	<b>6</b>
4.1	Mean speed . . . . .	6
4.2	Speed fluctuations . . . . .	7
<b>5</b>	<b>Correlation functions</b>	<b>7</b>
<b>6</b>	<b>Displacement</b>	<b>8</b>
6.1	Mean squared displacement . . . . .	9
6.2	Displacement fluctuations . . . . .	14
6.3	Components of displacement fluctuation . . . . .	17
6.3.1	Parallel component: . . . . .	17
6.3.2	Perpendicular component: . . . . .	18
<b>7</b>	<b>Fourth moment and kurtosis</b>	<b>20</b>
7.1	Fourth moment of speed . . . . .	20
7.2	Fourth moment of displacement . . . . .	20
7.3	Kurtosis: deviations from the Gaussian process . . . . .	21
<b>8</b>	<b>Discussion</b>	<b>23</b>
	<b>Appendix A</b>	<b>24</b>
	<b>Appendix B</b>	<b>25</b>

## 1. Introduction

Active matter consists of self-propelled units, each of which can consume and dissipate internal or ambient energy to maintain the system out of equilibrium and generate systematic motion [1, 2, 3, 4, 5]. The self-propulsion breaks the detailed balance condition and the equilibrium fluctuation-dissipation relation. Examples of self-propelled entities abound in nature, ranging from motor proteins [6, 7], bacteria [8, 9] to macro-scale entities like birds and animals [10]. Inspired by natural examples, several artificial active elements have been fabricated. This includes colloidal microswimmers, active rollers, vibrated rods, and asymmetric disks [2, 3]. Active colloids self-propel in their instantaneous heading direction through auto-catalytic drive utilizing ambient chemical, optical, thermal, or electric energy. They are typically modeled as active Brownian particles (ABP) with constant self-propulsion speed in a heading direction that undergoes orientational diffusion. Their long-time dynamics are similar to the run-and-tumble particles (RTP) [11] and the active Ornstein-Uhlenbeck process [12, 13]. Despite enormous progress in the knowledge of collective properties of active matter, the non-equilibrium nature of individual particles are yet to be completely understood. Recent studies showed that even non-interacting self-propelled particles can display rich and counterintuitive physical properties [14, 15, 16, 17, 18, 19, 20, 21, 22, 23, 24, 25, 26, 27, 28, 29, 30]. The RTP particles show a late-time condensation [29]. In the absence of thermal noise, exact short and long time properties of ABPs were obtained, and anisotropies in their short time motion were pointed out [17, 19, 23]. Such anisotropies survive even in the presence of thermal noise [21].

In a collection of ABPs with constant self-propulsion, collisions can lead to speed fluctuations [31, 32] impacting their motion. In active polymers, the speeds of individual bond segments and the center of mass undergo fluctuations due to bonding, bending, and self-avoidance [33, 34, 35, 21]. Moreover, the generation of self-propulsion, be it via auto-catalysis in active colloids or complex active processes in motile cells, involves internal stochastic processes that render inherent fluctuations to active speed [4, 36, 37, 38, 39, 40, 41, 42, 43, 44]. The RTP model with generic speed distributions has been studied recently [29, 45, 46, 47, 48]. Nevertheless, apart from few exceptions [37, 49, 4], in the most well studied ABP model, the active speed is taken to be constant.

In this paper, we reconsider the Schienbein-Gruler mechanism for active speed generation [36, 37]. This involves an Ornstein-Uhlenbeck process leading to speed fluctuations around a well-defined mean. The heading direction of self-propulsion undergoes orientational diffusion, as usual. In addition, we consider a translational thermal noise influencing the motion of ABPs. We extend and utilize a Fokker-Planck equation-based method [21, 50] to obtain arbitrary moments of the dynamics of speed-fluctuating ABPs in general  $d$ -dimensions. The presence of speed fluctuations and the competition between the speed relaxation time with other time scales, e.g., the persistence time, leads to new crossovers. The direct calculation presented here

allows for coevolution of active speed generation and spatial displacement. Our general result for mean squared displacement when interpreted for two-dimensions agrees with Ref. [36, 49] in the limit of fast relaxation of active speed, such that the steady-state limit of the speed correlation function can be used. We, in particular, analyze the changes in the physical properties of ABP due to speed fluctuations. The analysis shows an intermediate time regime of clear sub-diffusive scaling in the positional fluctuations parallel to the initial heading orientation, a behavior that disappears in the limit of constant active speed. The main achievements of this paper are the following: (i) We discuss a method for calculating the exact time-dependence of dynamical moments in arbitrary dimensions. We derive the expressions for the second and fourth moments of the displacement vector, its fluctuations, and fluctuations in its projection along the initial heading direction and in directions perpendicular to it. (ii) We show and analyze the presence of multiple crossovers in the mean-squared displacement and fluctuations of displacement vectors. (iii) In the intermediate time scales, the kurtosis of the displacement vector measuring the deviations from possible normal distributions changes between positive and negative values before returning to the Gaussian behavior at long times. Such deviations are controlled by the dominance of speed and orientational fluctuations, respectively.

The paper is organized as follows. In Section 2, we describe the model. In Section 3, we present the Laplace transform method starting from the Fokker-Planck equation to derive the general equation for calculating arbitrary moments of dynamical variables in  $d$ -dimensions. In the following Sections, we present calculations of particular quantities of interest: the mean speed and speed fluctuations in Section 4, the speed, orientation, and velocity auto-correlation functions in Section 5, and the mean-squared displacement and displacement fluctuations in Section 6. In Section 7, we calculate the fourth moment of displacement and the kurtosis to characterize the non-Gaussian nature of displacement fluctuations. The kurtosis shows positive and negative maxima in time corresponding to relaxations of speed and orientational fluctuations, respectively. Finally, in Section 8, we conclude by summarizing the main results.

## 2. Model

An active Brownian particle (ABP) with fluctuating speed in  $d$ -dimension is described by its position  $\mathbf{r} = (r_1, r_2, \dots, r_d)$  and active velocity  $\mathbf{v}$  having a scalar speed  $v$  in the orientation  $\hat{\mathbf{u}} = (u_1, u_2, \dots, u_d)$ , a  $d$ -dimensional unit vector that performs rotational diffusion on a unit sphere. The active speed  $v$  is determined by a Ornstein-Uhlenbeck process. In the presence of a translational Brownian noise the motion of the particle is describes within the Ito convention [51, 52, 53] as,

$$dr_i = v(t)u_i dt + dB_i^t(t), \quad (1)$$

$$dv = -\gamma_v(v - v_0) dt + dB^s(t), \quad (2)$$

$$du_i = (\delta_{ij} - u_i u_j) dB_j^r(t) - (d-1)D_r u_i dt. \quad (3)$$

Equation (1) describes the evolution of particle position due to time dependent active speed  $v(t)$  in orientation  $\hat{\mathbf{u}}(t)$ . The stochastic variables  $v(t)$  and  $\hat{\mathbf{u}}(t)$  evolve independently. The translational diffusion due to thermal noise is described by the Gaussian process  $d\mathbf{B}^t$  with mean zero and variance  $\langle dB_i^t dB_j^t \rangle = 2D\delta_{ij} dt$ .

Equation (2) describes the active speed generation following an Ornstein-Uhlenbeck process [36, 37], with mean speed relaxing to  $v_0$  in a time scale  $\gamma_v^{-1}$ . The Gaussian stochastic process  $dB^s$  obeys  $\langle dB^s(t) \rangle = 0$  and  $\langle dB^s dB^s \rangle = 2D_v dt$ , with  $D_v$  governing the speed fluctuations. Note that this process does not always ascertain a positive speed. A large  $D_v$  leads to larger fluctuations and as a result larger excursions towards negative speeds with respect to the heading direction. Here, it is instructive to note that such fluctuations of an effective negative speed can arise, e.g., in an assembly of repulsively interacting ABPs [31, 32] due to increased frontal collisions at larger particle density. In Appendix A, we discuss the dependence of cumulative speed distribution on the ratio  $D_v/\gamma_v$  for a given  $v_0$ .

Equation (3) represents the orientational diffusion of the heading direction. The Gaussian white noise  $d\mathbf{B}^r$  has zero mean and variance  $\langle dB_i^r dB_j^r \rangle = 2D_r \delta_{ij} dt$ . Alternatively, the equation can be expressed in the Stratonovich form  $du_i = (\delta_{ij} - u_i u_j) \circ dB_j^r(t)$ . Equation (3) ensures the normalization  $\mathbf{u}^2 = 1$  at all times.

We set  $\tau_r = 1/D_r$  as the unit of time, and  $\bar{\ell} = \sqrt{D/D_r}$  as the unit of length. All the speeds and velocities are expressed in units of  $\bar{v} = \bar{\ell}/\tau_r = \sqrt{DD_r}$ . The dimensionless quantities controlling speed-fluctuation and speed-relaxation are  $\tilde{D}_v = D_v \tau_r / \bar{v}^2 = D_v / DD_r^2$  and  $\tilde{\gamma}_v = \gamma_v / D_r$ . The mean active speed is expressed as a dimensionless Peclet number  $\text{Pe} = v_0 / \bar{v} = v_0 / \sqrt{DD_r}$ . It is straightforward to perform a direct numerical simulation of equations (1), (2), and (3) using the Euler-Maruyama integration to generate trajectories as illustrated in figure 1(a).

### 3. Calculation of moments from Fokker-Planck equation

In this Section, we present a general framework for the calculation of arbitrary moments of dynamical variables [21, 28]. The probability distribution  $P(\mathbf{r}, v, \hat{\mathbf{u}}, t)$  of the position  $\mathbf{r}$ , the speed  $v(t)$  and the heading direction  $\hat{\mathbf{u}}$  of the particle follows the Fokker-Planck equation

$$\partial_t P(\mathbf{r}, v, \hat{\mathbf{u}}, t) = D\nabla^2 P + D_r \nabla_u^2 P + D_v \partial_v^2 P - v \hat{\mathbf{u}} \cdot \nabla P + \gamma_v P + \gamma_v (v - v_0) \partial_v P \quad (4)$$

where  $\nabla$  is the  $d$ -dimensional Laplacian operator, and  $\nabla_u$  is the Laplacian in the  $(d-1)$  dimensional orientation space. In terms of the Laplace transform  $\tilde{P}(\mathbf{r}, v, \hat{\mathbf{u}}, s) = \int_0^\infty dt e^{-st} P(\mathbf{r}, v, \hat{\mathbf{u}}, t)$ , the Fokker-Planck equation takes the form,

$$-P(\mathbf{r}, v, \hat{\mathbf{u}}, 0) + (s - \gamma_v) \tilde{P}(\mathbf{r}, v, \hat{\mathbf{u}}, s) = D\nabla^2 \tilde{P} + D_r \nabla_u^2 \tilde{P} + D_v \partial_v^2 \tilde{P} - v \hat{\mathbf{u}} \cdot \nabla \tilde{P} + \gamma_v (v - v_0) \partial_v \tilde{P}.$$

Defining the mean of an observable  $\langle \psi \rangle_s = \int d\mathbf{r} dv d\hat{\mathbf{u}} \psi(\mathbf{r}, v, \hat{\mathbf{u}}) \tilde{P}(\mathbf{r}, v, \hat{\mathbf{u}}, s)$ , multiplying the above equation by  $\psi(\mathbf{r}, v, \hat{\mathbf{u}})$  and integrating over all possible  $(\mathbf{r}, v, \hat{\mathbf{u}})$  we obtain,

$$-\langle \psi \rangle_0 + s \langle \psi \rangle_s = D \langle \nabla^2 \psi \rangle_s + D_r \langle \nabla_u^2 \psi \rangle_s + D_v \langle \partial_v^2 \psi \rangle_s + \langle v \hat{\mathbf{u}} \cdot \nabla \psi \rangle_s - \gamma_v \langle (v - v_0) \partial_v \psi \rangle_s. \quad (5)$$

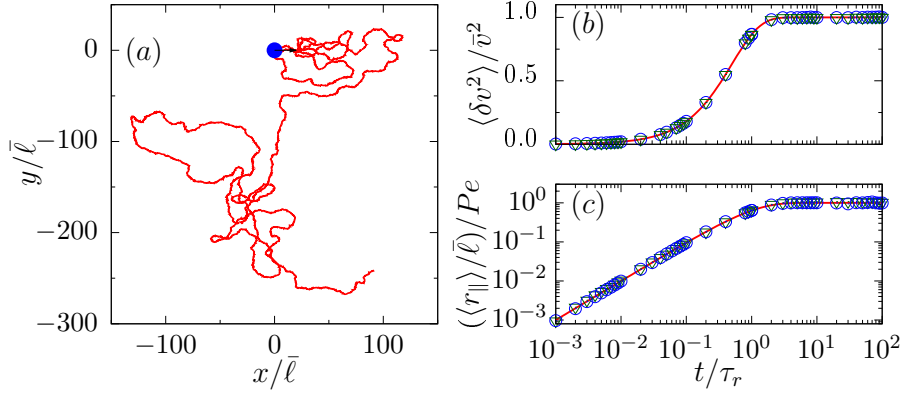


**Figure 1.** (color online) ABP in two-dimensions (2d) with  $\tilde{D}_v = 1$ , and  $\tilde{\gamma}_v = 1$ . (a) Typical ABP trajectories over a duration  $t = 100 \tau_r$  for  $Pe = 20$ . The blue point with arrow in each plot shows starting position and heading direction of the ABP. In these plots we used the initial active speed  $v_1 = \bar{v}Pe$  and heading direction  $\hat{\mathbf{u}}_0 = \hat{x}$  along the  $x$ -axis. (b) Scaled speed fluctuation  $\langle \delta v^2 \rangle / \bar{v}^2$  as a function of time  $t / \tau_r$  for  $Pe = 1$  (○),  $20$  (▽). The points are simulation results and the solid line is a plot of equation (8). (c) Displacement in the initial heading direction  $\langle r_{\parallel} \rangle$  as a function of time  $t$  for  $Pe = 1$  (○),  $20$  (▽). The points denote simulation results, and line depict  $\langle r_{\parallel} \rangle = \langle \mathbf{r} \rangle \cdot \hat{\mathbf{u}}_0$  using equation (15).

where, the initial condition sets  $\langle \psi \rangle_0 = \int d\mathbf{r} dv d\hat{\mathbf{u}} \psi(\mathbf{r}, v, \hat{\mathbf{u}}) P(\mathbf{r}, v, \hat{\mathbf{u}}, 0)$ . Without any loss of generality, we consider the initial condition  $P(\mathbf{r}, v, \hat{\mathbf{u}}, 0) = \delta(\mathbf{r}) \delta(v - v_1) \delta(\hat{\mathbf{u}} - \hat{\mathbf{u}}_0)$ , where  $v_1$  is an initial speed that, in general, is different from  $v_0$ . Equation (5) can be utilized to compute exact moments of any dynamical variable in  $d$ -dimensions as a function of time.

## 4. Active speed

In this Section, we first calculate the average active speed and speed fluctuations. We show how the speed fluctuations saturate over a long time. Next we calculate two-time auto-correlation functions for the heading direction, active speed, and velocity.

### 4.1. Mean speed

To calculate the evolution of active speed, we use  $\psi = v$  and the initial condition  $\langle \psi \rangle_0 = v_1$  in equation (5). Other terms required for the calculation are:  $\langle \nabla^2 \psi \rangle_s = 0$ ,  $\langle \nabla_{\hat{\mathbf{u}}}^2 \psi \rangle_s = 0$ ,  $\langle \partial_v^2 \psi \rangle_s = 0$ ,  $\langle v \hat{\mathbf{u}} \cdot \nabla \psi \rangle_s = 0$ ,  $\langle (v - v_0) \partial_v \psi \rangle_s = \langle v \rangle_s - v_0 \langle 1 \rangle_s = \langle v \rangle_s - v_0 / s$ . In the last relation we used  $\langle 1 \rangle_s = \int d\mathbf{r} d\hat{\mathbf{u}} dv \tilde{P} = \int d\mathbf{r} d\hat{\mathbf{u}} dv \int_0^\infty dt e^{-st} P = \int_0^\infty dt e^{-st} \{d\mathbf{r} d\hat{\mathbf{u}} dv P\} = \int_0^\infty dt e^{-st} = 1/s$ . Thus from equation (5), we get  $\langle v \rangle_s = v_1 / (s + \gamma_v) + v_0 \gamma_v / s (s + \gamma_v)$ . The inverse Laplace transform of this relation gives

$$\langle v \rangle(t) = v_1 e^{-\gamma_v t} + v_0 (1 - e^{-\gamma_v t}). \quad (6)$$

At the long time limit of  $\gamma_v t \gg 1$  this gives the steady state value  $\langle v \rangle = v_0$ .

#### 4.2. Speed fluctuations

To calculate speed fluctuations, we consider  $\psi = v^2$  and the initial condition  $\langle \psi \rangle_0 = v_1^2$  in equation (5). The other terms involved in the calculation are:  $\langle \nabla^2 \psi \rangle_s = 0$ ,  $\langle \nabla_u^2 \psi \rangle_s = 0$ ,  $\langle \partial_v^2 \psi \rangle_s = \langle 2 \rangle_s = 2/s$ ,  $\langle v \hat{\mathbf{u}} \cdot \nabla \psi \rangle_s = 0$ ,  $\langle (v - v_0) \partial_v \psi \rangle_s = 2 \langle v^2 \rangle_s - 2v_0 \langle v \rangle_s$ . Thus, we get from equation (5),  $\langle v^2 \rangle_s = (s + 2\gamma_v)^{-1} [v_1^2 + 2\gamma_v v_0 \langle v \rangle_s + 2D_v/s]$ . Its inverse Laplace transform gives

$$\langle v^2 \rangle(t) = [v_1 e^{-\gamma_v t} + v_0 (1 - e^{-\gamma_v t})]^2 + \frac{D_v}{\gamma_v} (1 - e^{-2\gamma_v t}). \quad (7)$$

As a result, using equation (6), the speed fluctuation can be expressed as,

$$\langle \delta v^2 \rangle = \langle v^2 \rangle - \langle v \rangle^2 = \frac{D_v}{\gamma_v} (1 - e^{-2\gamma_v t}). \quad (8)$$

This relation can be directly derived integrating equation (2) as is shown in equation (B.8) of Appendix B. In the long time limit of  $\gamma_v t \gg 1$ , the equation gives the steady state fluctuations  $\langle \delta v^2 \rangle = D_v/\gamma_v$ . A comparison of the prediction of equation (8) with simulation results is shown in figure 1(b).

### 5. Correlation functions

The evolution of heading direction  $\hat{\mathbf{u}}$  is an independent stochastic process, and thus does not get influenced by the speed fluctuations. Using equation (B.8) one can show that the persistence of heading direction decays as  $\langle \hat{\mathbf{u}}(t) \rangle = \hat{\mathbf{u}}_0 e^{-(d-1)D_r t}$  and as a result the correlation

$$\langle \hat{\mathbf{u}}(t) \cdot \hat{\mathbf{u}}(0) \rangle = e^{-(d-1)D_r t}, \quad (9)$$

as was shown in Ref. [21]. The auto-correlation function of active speed can be directly calculated from equation (2) as is shown in Appendix B,

$$\langle \delta v(t_1) \delta v(t_2) \rangle = \frac{D_v}{\gamma_v} [e^{-\gamma_v |t_1 - t_2|} - e^{-\gamma_v (t_1 + t_2)}], \quad (10)$$

where  $\delta v(t) = v(t) - \langle v(t) \rangle$ . In the steady state limit of  $t_1, t_2 \rightarrow \infty$ , writing the time gap  $\tau = |t_1 - t_2|$  one gets the simplified expression

$$\langle \delta v(\tau) \delta v(0) \rangle = (D_v/\gamma_v) e^{-\gamma_v \tau}. \quad (11)$$

The velocity correlation can be calculated directly from the Langevin equations writing  $\dot{\mathbf{r}} = \mathbf{v}$ . This gives  $\langle \mathbf{v}(t) \rangle = \langle v(t) \rangle \langle \hat{\mathbf{u}}(t) \rangle$  and  $\langle \mathbf{v}(t_1) \cdot \mathbf{v}(t_2) \rangle = \langle v(t_1) v(t_2) \rangle \langle \hat{\mathbf{u}}(t_1) \cdot \hat{\mathbf{u}}(t_2) \rangle + 2D\delta(t_1 - t_2)$ . Thus, a direct calculation leads to

$$\langle \mathbf{v}(t_1) \cdot \mathbf{v}(t_2) \rangle = \left[ \frac{D_v}{\gamma_v} (e^{-\gamma_v (t_1 - t_2)} - e^{-\gamma_v (t_1 + t_2)}) + \langle v(t_1) \rangle \langle v(t_2) \rangle \right] e^{-(d-1)D_r (t_1 - t_2)} + 2D\delta(t_1 - t_2) \quad (12)$$

The decay of velocity correlation is dictated by two time constants, the speed correlation time  $\gamma_v^{-1}$  and the persistence time of the heading direction  $D_r^{-1}$ . The autocorrelation between fluctuations of velocity  $\delta\mathbf{v}(t) = \mathbf{v}(t) - \langle\mathbf{v}(t)\rangle$  is given by  $\langle\delta\mathbf{v}(t_1)\delta\mathbf{v}(t_2)\rangle$ . Note that the mean velocity at time  $t$  is given by  $\langle\mathbf{v}(t)\rangle = \langle v(t)\rangle\langle\hat{\mathbf{u}}(t)\rangle$ , where  $\langle v(t)\rangle$  is given by equation (6) and  $\langle\hat{\mathbf{u}}(t)\rangle = \hat{\mathbf{u}}_0 e^{-(d-1)D_r t}$ . Therefore,  $\langle\mathbf{v}(t)\rangle = [v_1 e^{-\gamma_v t} + v_0(1 - e^{-\gamma_v t})]\hat{\mathbf{u}}_0 e^{-(d-1)D_r t}$ . The expression simplifies in the steady state limit in which  $\langle v(t)\rangle = v_0$ , using  $t_1, t_2 \rightarrow \infty$  and writing  $t_1 - t_2 = \tau$  one gets

$$\langle\delta\mathbf{v}(\tau)\delta\mathbf{v}(0)\rangle = \left[ v_0^2 + \frac{D_v}{\gamma_v} e^{-\gamma_v \tau} \right] e^{-(d-1)D_r \tau} + 2D\delta(\tau). \quad (13)$$

## 6. Displacement

In this Section, we compute various moments of the displacement vector using equation (5). We begin by setting  $\psi = \mathbf{r}$ , and initial location  $\langle\psi\rangle_0 = \mathbf{0}$  at the origin. The calculation uses  $\langle\nabla^2\psi\rangle_s = 0$ ,  $\langle\nabla_u^2\psi\rangle_s = 0$ ,  $\langle\partial_v^2\psi\rangle_s = 0$ ,  $\langle v\hat{\mathbf{u}} \cdot \nabla\psi\rangle_s = \langle v\hat{\mathbf{u}}\rangle_s$ , and  $\langle(v - v_0)\partial_v\psi\rangle_s = 0$  in equation (5). This gives  $\langle\mathbf{r}\rangle_s = \langle v\hat{\mathbf{u}}\rangle_s/s$ . Again, the same equation (5) gives  $\langle v\hat{\mathbf{u}}\rangle_s = \frac{1}{s + \gamma_v + (d-1)D_r} [v_1\hat{\mathbf{u}}_0 + \gamma_v v_0\langle\hat{\mathbf{u}}\rangle_s]$  and  $\langle\hat{\mathbf{u}}\rangle_s = \hat{\mathbf{u}}_0/(s + (d-1)D_r)$ . Therefore, we get

$$\langle\mathbf{r}\rangle_s = \frac{(v_1 - v_0)\hat{\mathbf{u}}_0}{s(s + (d-1)D_r + \gamma_v)} + \frac{v_0\hat{\mathbf{u}}_0}{s(s + (d-1)D_r)}. \quad (14)$$

Performing the inverse Laplace transform this leads to the evolution of the displacement vector

$$\langle\mathbf{r}\rangle(t) = \frac{(v_1 - v_0)\hat{\mathbf{u}}_0}{(d-1)D_r + \gamma_v} (1 - e^{-((d-1)D_r + \gamma_v)t}) + \frac{v_0\hat{\mathbf{u}}_0}{(d-1)D_r} (1 - e^{-(d-1)D_r t}). \quad (15)$$

In Figure 1(c) we show a comparison of this estimate of displacement in the direction of the initial heading direction  $\langle r_{\parallel}\rangle = \langle\mathbf{r}\rangle \cdot \hat{\mathbf{u}}_0$  as obtained from equation (15) with numerical simulations.

**Position-orientation cross-correlation  $\langle\hat{\mathbf{u}} \cdot \mathbf{r}\rangle$ :** Calculation of higher moments of displacement vector involves this equal time cross-correlation. We set  $\psi = \hat{\mathbf{u}} \cdot \mathbf{r}$  and the initial condition  $\langle\psi\rangle_0 = 0$  in equation (5). The calculation uses the relations:  $\langle\nabla^2\psi\rangle_s = 0$ ,  $\langle\nabla_u^2\psi\rangle_s = -(d-1)D_r\langle\hat{\mathbf{u}} \cdot \mathbf{r}\rangle_s$ ,  $\langle\partial_v^2\psi\rangle_s = 0$ ,  $\langle v\hat{\mathbf{u}} \cdot \nabla\psi\rangle_s = \langle v\rangle_s$ , and  $\langle(v - v_0)\partial_v\psi\rangle_s = 0$ . As a result, one gets  $\langle\hat{\mathbf{u}} \cdot \mathbf{r}\rangle_s = \langle v\rangle_s/(s + (d-1)D_r)$ . To completely determine the cross-correlation in the Laplace space, we utilize equation (5) further to obtain  $\langle v\rangle_s = v_1/(s + \gamma_v) + \gamma_v v_0/s(s + \gamma_v)$ . These results lead to

$$\langle\hat{\mathbf{u}} \cdot \mathbf{r}\rangle_s = \frac{v_1 - v_0}{(s + \gamma_v)(s + (d-1)D_r)} + \frac{v_0}{s(s + (d-1)D_r)}. \quad (16)$$

The inverse Laplace transform of equation (16) gives

$$\langle\hat{\mathbf{u}} \cdot \mathbf{r}\rangle(t) = \frac{v_1 - v_0}{(d-1)D_r - \gamma_v} (e^{-\gamma_v t} - e^{-(d-1)D_r t}) + \frac{v_0}{(d-1)D_r} (1 - e^{-(d-1)D_r t}). \quad (17)$$

It is interesting to note that for initial active speed  $v_1 = v_0$ , the cross-correlation reduces to  $\langle\hat{\mathbf{u}} \cdot \mathbf{r}\rangle(t) = v_0(1 - e^{-(d-1)D_r t})/(d-1)D_r$ , an expression that is the same as ABPs in the absence of active speed fluctuations as described in Ref. [21].

### 6.1. Mean squared displacement

Here we present an exact computation of the mean squared displacement  $\langle \mathbf{r}^2 \rangle$ . We use  $\psi = \mathbf{r}^2$  and the initial condition  $\langle \mathbf{r}^2 \rangle_0 = 0$  in equation (5). The calculation of the moment uses the relations  $\langle \nabla_u^2 \mathbf{r}^2 \rangle_s = 0$ ,  $\langle \nabla^2 \mathbf{r}^2 \rangle_s = 2d/s$  and  $\langle v \hat{\mathbf{u}} \cdot \nabla \mathbf{r}^2 \rangle_s = 2\langle v \hat{\mathbf{u}} \cdot \mathbf{r} \rangle_s$ . Thus equation (5) leads to

$$\langle \mathbf{r}^2 \rangle_s = \frac{1}{s} \left[ \frac{2dD}{s} + 2\langle v \hat{\mathbf{u}} \cdot \mathbf{r} \rangle_s \right]. \quad (18)$$

To complete the calculation, one needs to evaluate  $\langle v \hat{\mathbf{u}} \cdot \mathbf{r} \rangle_s$ , again, using the same equation (5). One may proceed like before, using  $\psi = v \hat{\mathbf{u}} \cdot \mathbf{r}$  and  $\langle \psi \rangle_0 = 0$ ,  $\langle \nabla^2 \psi \rangle_s = 0$ ,  $\langle \nabla_u^2 (v \hat{\mathbf{u}} \cdot \mathbf{r}) \rangle_s = -(d-1)\langle v \hat{\mathbf{u}} \cdot \mathbf{r} \rangle_s$ ,  $\langle v \hat{\mathbf{u}} \cdot \nabla (v \hat{\mathbf{u}} \cdot \mathbf{r}) \rangle_s = \langle v^2 \hat{\mathbf{u}}^2 \rangle_s = \langle v^2 \rangle_s$  to obtain

$$\langle v \hat{\mathbf{u}} \cdot \mathbf{r} \rangle_s = \frac{1}{(s + (d-1)D_r + \gamma_v)} [\langle v^2 \rangle_s + \gamma_v v_0 \langle \hat{\mathbf{u}} \cdot \mathbf{r} \rangle_s].$$

Similar calculations give,

$$\begin{aligned} \langle v^2 \rangle_s &= \frac{1}{s + 2\gamma_v} \left[ v_1^2 + 2D_v \langle 1 \rangle_s + \frac{2\gamma_v v_0}{s + \gamma_v} [v_1 + \gamma_v v_0 \langle 1 \rangle_s] \right], \\ \langle \hat{\mathbf{u}} \cdot \mathbf{r} \rangle_s &= \frac{v_1 - v_0}{(s + \gamma_v)(s + (d-1)D_r)} + \frac{v_0}{s(s + (d-1)D_r)}. \end{aligned}$$

Thus, plugging these relations back in the expression of  $\langle \mathbf{r}^2 \rangle_s$  in equation (18), we obtain

$$\begin{aligned} \langle \mathbf{r}^2 \rangle_s &= \frac{2dD}{s^2} + \frac{4D_v}{s^2(s + 2\gamma_v)(s + (d-1)D_r + \gamma_v)} \\ &+ \frac{2\gamma_v v_0}{s(s + (d-1)D_r)(s + \gamma_v)(s + (d-1)D_r + \gamma_v)} \left( v_1 + \frac{\gamma_v v_0}{s} \right) \\ &+ \frac{2}{s(s + (d-1)D_r + \gamma_v)(s + 2\gamma_v)} \left[ v_1^2 + \frac{2\gamma_v v_0}{(s + \gamma_v)} \left( v_1 + \frac{\gamma_v v_0}{s} \right) \right] \end{aligned} \quad (19)$$

Performing the inverse Laplace transform, this leads to

$$\begin{aligned} \langle \mathbf{r}^2 \rangle &= \frac{(D_v - \gamma_v(v_0 - v_1)^2) e^{-2\gamma_v t}}{\gamma_v^2((d-1)D_r - \gamma_v)} + \frac{2(2(d-1)D_r - \gamma_v)v_0(v_0 - v_1)e^{-\gamma_v t}}{(d-1)D_r\gamma_v((d-1)D_r - \gamma_v)} \\ &+ \frac{2(-\gamma_v^2 v_0^2 + (d-1)D_r\gamma_v v_0 v_1) e^{-(d-1)D_r t}}{(d-1)^2 D_r^2 ((d-1)D_r - \gamma_v)\gamma_v} \\ &+ \frac{2((d-1)^2 d D D_r^2 \gamma_v + \gamma_v^2 v_0^2 + (d-1)D_r (D_v + \gamma_v (d D \gamma_v + v_0^2))) t}{(d-1)D_r\gamma_v((d-1)D_r + \gamma_v)} \\ &+ \frac{2(d-1)D_r\gamma_v^3 v_0(-3v_0 + v_1) - 2\gamma_v^4 v_0^2}{(d-1)^2 D_r^2 \gamma_v^2 ((d-1)D_r + \gamma_v)^2} \\ &- \frac{(d-1)^3 D_r^3 (D_v + \gamma_v(v_0 - v_1)(3v_0 + v_1)) + (d-1)^2 D_r^2 \gamma_v (3D_v + \gamma_v (7v_0^2 - 4v_0 v_1 - v_1^2))}{(d-1)^2 D_r^2 \gamma_v^2 ((d-1)D_r + \gamma_v)^2} \\ &- \frac{2((d-1)D_r\gamma_v(2D_v - \gamma_v(v_0 - v_1)(v_0 - v_1))) e^{-((d-1)D_r + \gamma_v)t}}{(d-1)D_r((d-1)D_r - \gamma_v)\gamma_v((d-1)D_r + \gamma_v)^2} \\ &- \frac{2((d-1)^2 D_r^2 \gamma_v (v_0 - v_1)v_1 + \gamma_v^3 v_0(-v_0 + v_1)) e^{-((d-1)D_r + \gamma_v)t}}{(d-1)D_r((d-1)D_r - \gamma_v)\gamma_v((d-1)D_r + \gamma_v)^2} \end{aligned} \quad (20)$$

The derivation of  $\langle \mathbf{r}^2 \rangle$  in  $d$ -dimensions shown in equation (20) is our first main result. Considering the initial active speed  $v_1 = v_0$ , equation (20) simplifies to

$$\begin{aligned} \langle \mathbf{r}^2 \rangle = & 2dDt + \frac{2v_0^2}{(d-1)D_r} \left( t - \frac{1 - e^{-(d-1)D_r t}}{(d-1)D_r} \right) \\ & + \frac{2D_v}{\gamma_v(\gamma_v + (d-1)D_r)} \left( t - \frac{1 - e^{-(\gamma_v + (d-1)D_r)t}}{\gamma_v + (d-1)D_r} \right) \\ & - \frac{2D_v}{\gamma_v(\gamma_v + (d-1)D_r)} \left[ \frac{1 - e^{-2\gamma_v t}}{2\gamma_v} - \frac{e^{-2\gamma_v t} - e^{-(\gamma_v + (d-1)D_r)t}}{\gamma_v - (d-1)D_r} \right]. \end{aligned} \quad (21)$$

Note that for the special case of  $(d-1)D_r = \gamma_v$ , equation (21) can be further simplified by using the L'Hôpital's rule, or, directly substituting  $(d-1)D_r = \gamma_v$  and  $v_1 = v_0$  in equation (19) to calculate  $\langle \mathbf{r}^2 \rangle$ .

In the limits of  $D_v \rightarrow 0$  and  $\gamma_v \rightarrow \infty$ , equation (21) reduces to that of free ABPs in the absence of speed fluctuations, as shown in Ref. [21]. The structure of the second and third terms in equation (21) can describe two ballistic diffusive crossovers [49]. As we show in the following, the presence of the fourth term allows for further crossovers. Moreover, the presence of translational diffusion makes the short time dynamics diffusive. Here, it is instructive to note that the calculations of lower moments can be performed easily using the Langevin equations. For example, the formal solution for the position vector,  $\mathbf{r}(t) = \int_0^t dt' v(t') \hat{\mathbf{u}}(t') + \int_0^t d\mathbf{B}^t(t')$  leads to the second moment

$$\langle \mathbf{r}^2 \rangle = \int_0^t dt_1 \int_0^t dt_2 \langle v(t_1)v(t_2) \rangle \langle \hat{\mathbf{u}}(t_1) \cdot \hat{\mathbf{u}}(t_2) \rangle + \int_0^t \int_0^t \langle d\mathbf{B}^t(t_1) \cdot d\mathbf{B}^t(t_2) \rangle, \quad (22)$$

where the cross terms do not appear as they describe independent stochastic processes with  $\langle d\mathbf{B}^t \rangle = 0$ . By substituting the speed correlation function from equation (10) and the orientational correlation function from equation (9) in equation (22), and performing the integrations, one gets the same mean squared displacement relation as in equation (21).

In figure2 we compare our analytic prediction for the second moment of displacement shown in equation (21) with direct numerical simulation results in 2d ( $d = 2$ ) to find excellent agreement between them. Here, it is instructive to note the difference of our  $d$ -dimensional expression for  $\langle \mathbf{r}^2 \rangle$  shown in equation (21) from earlier results for 2d obtained in Ref. [36, 49]. The difference stems from an assumption of time-scale separation used in these earlier publications, where the speed fluctuations were assumed to be in steady state. This can be easily seen by noting that instead of using the general result for  $\langle v(t_1)v(t_2) \rangle$  of equation (10), if one uses the steady state limit of the correlation for active speed as in equation (11), the expression in equation (22) leads to the previously obtained relation for the second moment of displacement [36, 49]

$$\langle \mathbf{r}^2 \rangle = 4Dt + 2v_0^2 \left( \frac{t}{D_r} - \frac{1 - e^{-D_r t}}{D_r^2} \right) + \frac{2D_v}{\gamma_v} \left( \frac{t}{(\gamma_v + D_r)} - \frac{1 - e^{-(\gamma_v + D_r)t}}{(\gamma_v + D_r)^2} \right). \quad (23)$$

As is clearly shown in figure2, while our calculation in equation (21) exactly captures the behavior observed in numerical simulations, the earlier result shown in equation (23)

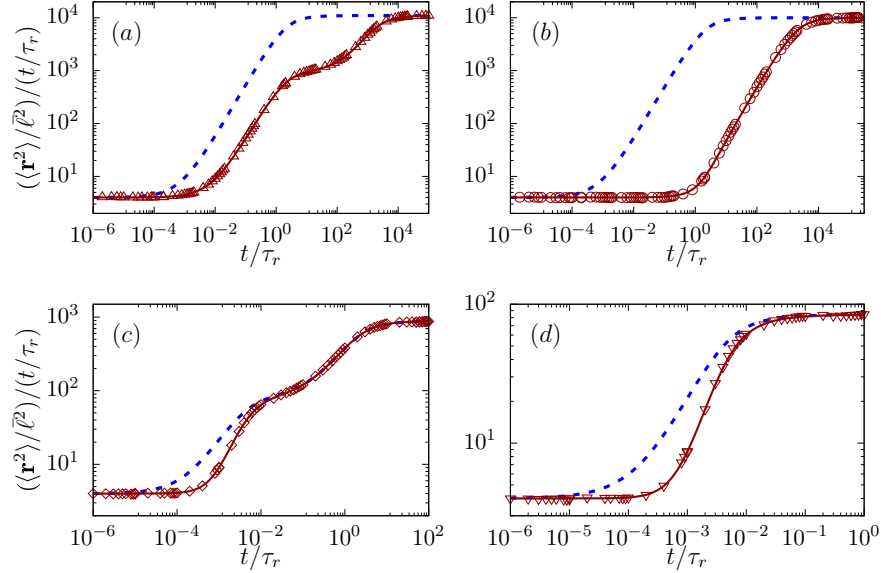


**Figure 2.** (color online) Time dependence of  $\langle \mathbf{r}^2 \rangle / t$  in 2d. The slow and fast relaxations of active speed are considered in (a,b)  $\tilde{\gamma}_v \ll 1$ , and (c,d)  $\tilde{\gamma}_v \gg 1$ , respectively. The points denote simulation results, the solid lines depict equation (21) with  $d = 2$ , and the dashed lines depict equation (23). Parameter values used in (a,b):  $\tilde{\gamma}_v = 5 \times 10^{-4}$ ,  $\tilde{D}_v = 2.5$  with  $Pe = 22.36$  (a) and 1.12 (b). Parameter values used in (c,d):  $\tilde{\gamma}_v = 5 \times 10^2$ ,  $\tilde{D}_v = 10^7$  with  $Pe = 20$  (c) and 1 (d). Initial conditions are chosen such as the active speed speed  $v_1/\bar{v} = Pe$  and the heading direction  $\hat{\mathbf{u}}_0 = \hat{x}$  is along the  $x$ -axis.

deviates from the numerically obtained  $\langle \mathbf{r}^2 \rangle(t)$ . In figure 2, the qualitative difference can be seen clearly at small  $\tilde{\gamma}_v/D_r$  and large  $Pe$ . The figure shows multiple ballistic diffusive crossovers, which we describe in detail in the following.

**Multiple crossovers and crossover timescales:** To elucidate the crossovers permitted by equation (21), we focus on its behavior in different time regimes. First, we note that in the two limits of the shortest and longest times  $\langle \mathbf{r}^2 \rangle$  shows diffusive behavior, albeit with two significantly different diffusion constants. In the short time limit

$$\langle \mathbf{r}^2 \rangle \approx 2dDt \quad (24)$$

and in the long time limit

$$\langle \mathbf{r}^2 \rangle \approx 2d \left[ D + \frac{v_0^2}{d(d-1)D_r} + \frac{D_v}{d\tilde{\gamma}_v[\tilde{\gamma}_v + (d-1)D_r]} \right] t. \quad (25)$$

For the smallest time scales, we expand  $\langle \mathbf{r}^2 \rangle$  in equation (21) around  $t = 0$  to obtain

$$\langle \mathbf{r}^2 \rangle = 2dDt + v_0^2 t^2 - \frac{1}{3} ((d-1)D_r v_0^2 - 2D_v) t^3 + \mathcal{O}(t^4). \quad (26)$$

This shows a crossover from diffusive  $\langle \mathbf{r}^2 \rangle \sim t$  to ballistic behavior  $\langle \mathbf{r}^2 \rangle \sim t^2$  at  $t_I = 2dD/v_0^2$ , with the crossover point obtained by comparing the first and second terms

of the above expansion. Such crossovers have been observed in figure 2. Comparing the second and third terms in the above expansion, one can identify a possible second crossover from ballistic to diffusive behavior at  $t_{II} = 3v_0^2/[(d-1)D_r v_0^2 - 2D_v]$ , provided  $(d-1)D_r v_0^2 > 2D_v$ . Further insights can be drawn by separately considering the limits of (i) slow speed relaxation and (ii) slow orientational relaxation, separately.

(i) **Slow relaxation of active speed;  $\gamma_v \ll (d-1)D_r$  :** Using  $(d-1)D_r t \gg 1$  and  $2\gamma_v t \ll 1$ , we can write  $\exp[-(d-1)D_r t] \approx 0$ ,  $\exp[-((d-1)D_r + \gamma_v)t] \approx 0$  and expand  $\exp(-2\gamma_v t)$  around  $2\gamma_v t = 0$  in equation (21) to get

$$\langle \mathbf{r}^2 \rangle = \left( 2dD + \frac{2v_0^2}{(d-1)D_r} + \frac{4D_v}{(d-1)^2 D_r^2 - \gamma_v^2} \right) t + \frac{2D_v}{(d-1)D_r - \gamma_v} t^2 + \mathcal{O}(t^3). \quad (27)$$

This implies a possible third crossover  $\langle \mathbf{r}^2 \rangle \sim t$  to  $\sim t^2$  expected at  $t_{III} \sim [2dD + 2v_0^2/(d-1)D_r + 4D_v/((d-1)^2 D_r^2 - \gamma_v^2)] [(d-1)D_r - \gamma_v]/2D_v$ . The final crossover point to the long-time diffusive limit denoted by equation (25) can be calculated by comparing the last term in equation (27) with equation (25). This crossover time turns out to be  $t_{IV} \sim [2dD + 2v_0^2/(d-1)D_r + 2D_v/\gamma_v((d-1)D_r + \gamma_v)] [(d-1)D_r - \gamma_v]/2D_v$ .

Moreover, at small  $Pe$ , the diffusive-ballistic crossover at  $t_I$  can be preempted by a different ballistic-diffusive crossover at  $t_I^*$  that can be determined by comparing the first term in equation (26) with the second term in equation (27). This gives  $t_I^* = dD[(d-1)D_r - \gamma_v]/D_v$ , a crossover point independent of the active speed  $v_0$ .

Such crossovers for  $\langle \mathbf{r}^2 \rangle$  in 2d, in the limit of  $\gamma_v \tau_r \ll 1$ , are illustrated in figure 3.(a). The graphs depict the expression in equation (21) using parameter values  $\tilde{\gamma}_v = \gamma_v \tau_r = 5 \times 10^{-4}$ ,  $\tilde{D}_v = D_v \tau_r / \bar{v}^2 = 2.5$ . The solid line at larger  $Pe (= 22.36)$  shows all four diffusive- ballistic- diffusive crossovers discussed above, as the requirement  $t_I < t_{II} < t_{III} < t_{IV}$  is satisfied. In this case, the crossover times are  $t_I/\tau_r \sim 4/Pe^2 \approx 0.008$ ,  $t_{II}/\tau_r = 3Pe^2/(Pe^2 - 2\tilde{D}_v) \approx 3.03$ ,  $t_{III}/\tau_r = [4 + 2Pe^2 + 4\tilde{D}_v/(1 - \tilde{\gamma}_v^2)](1 - \tilde{\gamma}_v)/2\tilde{D}_v \approx 202.8$ , and  $t_{IV}/\tau_r = [4 + 2Pe^2 + 2\tilde{D}_v/\{\tilde{\gamma}_v(1 + \tilde{\gamma}_v)\}](1 - \tilde{\gamma}_v)/2\tilde{D}_v \approx 2200$ , as pointed out in figure 3(a).

For  $Pe = v_0/\bar{v} = 1.12$ ,  $\langle \mathbf{r}^2 \rangle$  denoted by the dashed line in figure 3.(a) shows only two crossovers: (a) a diffusive-ballistic crossover at  $t_I^*/\tau_r = 2(1 - \tilde{\gamma}_v)/\tilde{D}_v = 0.8$  and (b) a ballistic-diffusive crossover at  $t_{IV}/\tau_r \approx 2000$ . In this case  $t_I^* < t_I = 3.2\tau_r$ , thus the first diffusive-ballistic crossover is preempted by  $t_I^*$ . Other possible intermediate crossovers disappear due to the following reasons. The possible ballistic-diffusive crossover point  $t_{II} < 0$  for these parameters. In its absence, the point  $t_{III} \approx 3.3\tau_r$  signifying a possible diffusive-ballistic crossover cannot show any change in the already ballistic property of the ABP in that time regime.

(ii) **Fast relaxation of active speed;  $\gamma_v \gg (d-1)D_r$  :** The scenario of short-time diffusive-ballistic crossover at  $t_I = 2dD/v_0^2$  remains unchanged. As indicated before, at  $t_{II} = 3v_0^2/((d-1)D_r v_0^2 - 2D_v)$  with  $2D_v > (d-1)D_r v_0^2$ , a possible second crossover from  $\langle \mathbf{r}^2 \rangle \sim t^2$  to  $\langle \mathbf{r}^2 \rangle \sim t^3$  can appear. In the limit of  $(d-1)D_r t \ll 1$  and  $2\gamma_v t \gg 1$ , we can use  $\exp(-2\gamma_v t) \approx 0$ ,  $\exp[-((d-1)D_r + \gamma_v)t] \approx 0$  and expand  $\exp[-(d-1)D_r t]$  around

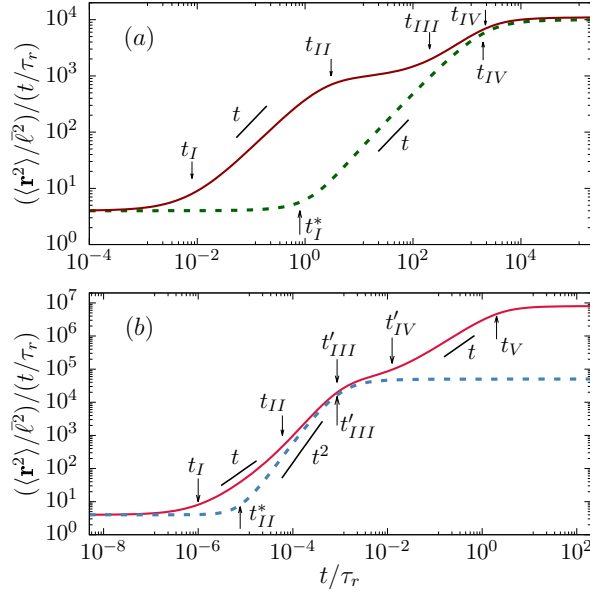


**Figure 3.** (color online) Persistent motion. Mean squared displacement  $\langle \mathbf{r}^2 \rangle$  as in equation (21) as a function of time  $t$  in two dimension,  $d = 2$ . (a) Parameters used are  $\tilde{\gamma}_v = 5 \times 10^{-4}$ ,  $\tilde{D}_v = 2.5$  with  $Pe = 22.36$  (solid line), 1.12 (dashed line). The solid line shows four crossover with crossover times  $t_I/\tau_r = 0.008$ ,  $t_{II}/\tau_r = 3.03$ ,  $t_{III}/\tau_r = 202.8$  and  $t_{IV}/\tau_r = 2200$ . The dashed line shows two crossovers: : a diffusive-ballistic crossover at  $t_I^*/\tau_r = 0.8$  and a ballistic-diffusive crossover at  $t_{IV}/\tau_r = 2000$ . (b) Parameters used are  $\tilde{\gamma}_v = 2 \times 10^3$ ,  $\tilde{D}_v = 10^{11}$ , with  $Pe = 2 \times 10^3$  (solid line), 10 (dashed line). The solid line shows five crossover with crossover times  $t_I/\tau_r = 10^{-6}$ ,  $t_{II}/\tau_r = 6 \times 10^{-5}$ ,  $t'_{III}/\tau_r = 8.6 \times 10^{-4}$  and  $t'_{IV}/\tau_r = 1.25 \times 10^{-2}$ , and  $t_V = 2.02$ . The dashed line shows two crossovers with crossover times  $t_I^*/\tau_r = 7.75 \times 10^{-6}$  and  $t'_{III}/\tau_r = 8.6 \times 10^{-4}$ . Initial activity: speed  $v_1/\bar{v} = Pe$  and heading direction along  $x$ -axis,  $\hat{\mathbf{u}}_0 = \hat{x}$ .

$D_r t = 0$  in equation (21) to get

$$\langle \mathbf{r}^2 \rangle = \left( 2dD + \frac{2D_v}{\gamma_v((d-1)D_r + \gamma_v)} \right) t + v_0^2 t^2 + \mathcal{O}(t^3). \quad (28)$$

Comparing the third term in equation (26) and the first term in equation (28), we estimate the crossover time from  $\langle \mathbf{r}^2 \rangle \sim t^3$  to  $\langle \mathbf{r}^2 \rangle \sim t$  to be at  $t'_{III} = \left[ 3 \frac{2dD + 2D_v/\{\gamma_v((d-1)D_r + \gamma_v)\}}{2D_v - (d-1)D_r v_0^2} \right]^{1/2}$ . Equation (28) suggests a fourth crossover from  $\langle \mathbf{r}^2 \rangle \sim t$  to  $\langle \mathbf{r}^2 \rangle \sim t^2$  at  $t'_{IV} = (2dD + 2D_v/(\gamma_v((d-1)D_r + \gamma_v)))/v_0^2$ . The final ballistic-diffusive crossover with  $(d-1)D_r \ll 2\gamma_v$  can be obtained by comparing the second term in equation (28) with equation (25). This gives the final crossover time  $t_V = (2dD + 2v_0^2/(d-1)D_r + 2D_v/\gamma_v((d-1)D_r + \gamma_v))/v_0^2$ .

There is also a possibility of getting a direct crossover from  $\langle \mathbf{r}^2 \rangle \sim t$  to  $\langle \mathbf{r}^2 \rangle \sim t^3$  at  $t_{II}^* = [6dD/(2D_v - (d-1)D_r v_0^2)]^{1/2}$  if  $t_{II}^* < t_I$ . The crossover point  $t_{II}^*$  is obtained by comparing the first and the third term of equation (26). Another direct final crossover from  $\langle \mathbf{r}^2 \rangle \sim t^3$  to  $\langle \mathbf{r}^2 \rangle \sim t$  can appear at  $t_{VI} = \{6d[D + \frac{v_0^2}{d(d-1)D_r} + \frac{D_v}{d\gamma_v[\gamma_v + (d-1)D_r]}\} / [2D_v -$

$(d-1)D_r v_0^2\}}^{1/2}$  if  $t_{VI} < t'_{III}$ , otherwise the final crossover will be at  $t'_{III}$ . The estimate of  $t_{VI}$  is obtained by comparing the third term in equation (26) with equation (25).

Such crossovers for  $\langle \mathbf{r}^2 \rangle$  in 2d in the limit of  $\gamma_v \tau_r \gg 1$  are illustrated in figure 3.(b). The graphs depict the expression in equation (21) using parameter values  $\tilde{\gamma}_v = \gamma_v \tau_r = 2 \times 10^3$ ,  $\tilde{D}_v = D_v \tau_r / \bar{v}^2 = 10^{11}$ . The solid line at  $Pe = v_0 / \bar{v} = 2 \times 10^3$  exhibits all five possible crossovers from  $\langle \mathbf{r}^2 \rangle \sim t$  to  $\sim t^2$ , to  $\sim t^3$ , to  $\sim t$ , to  $\sim t^2$  to finally  $\sim t$  as the requirement  $t_I < t_{II} < t'_{III} < t'_{IV} < t_V$  is satisfied. The crossover times are  $t_I / \tau_r \sim 4 / Pe^2 = 1 \times 10^{-6}$ ,  $t_{II} / \tau_r \sim 3Pe^2 / (Pe^2 - 2\tilde{D}_v^2) \approx 6 \times 10^{-5}$ ,  $t'_{III} / \tau_r = \left[ 3 \left( 4 + 2\tilde{D}_v / \{\tilde{\gamma}_v(1 + \tilde{\gamma}_v)\} \right) / (2\tilde{D}_v - Pe^2) \right]^{1/2} \approx 8.6 \times 10^{-4}$ ,  $t'_{IV} / \tau_r = [4 + 2\tilde{D}_v / \{\tilde{\gamma}_v(1 + \tilde{\gamma}_v)\}] / Pe^2 \approx 1 \times 10^{-2}$ ,  $t_V / \tau_r = [4 + 2Pe^2 + 2\tilde{D}_v / \{\tilde{\gamma}_v(1 + \tilde{\gamma}_v)\}] / Pe^2 \approx 2$ . They are identified by arrows on the solid line in figure 3(b).

For  $Pe = v_0 / \bar{v} = 10$ ,  $\langle \mathbf{r}^2 \rangle$  denoted by the dashed line in figure 3(b) shows only two crossovers: the first from  $\langle \mathbf{r}^2 \rangle \sim t$  to  $\langle \mathbf{r}^2 \rangle \sim t^3$  at  $t_{II}^*$ , and the second going back to  $\langle \mathbf{r}^2 \rangle \sim t$  at  $t_{VI}$ . Here,  $t_{II}^* / \tau_r = [12 / (2\tilde{D}_v - Pe^2)]^{1/2} \approx 7.75 \times 10^{-6}$  as  $t_{II}^* < t_I \approx 0.04 \tau_r$ . The  $\langle \mathbf{r}^2 \rangle \sim t^3$  to  $\langle \mathbf{r}^2 \rangle \sim t$  crossover appears at  $t'_{III} / \tau_r \approx 8.6 \times 10^{-4}$ , as  $t_{VI} / \tau_r = \left[ 12 \times \frac{1 + \frac{Pe^2}{2} + \frac{\tilde{D}_v}{\tilde{\gamma}_v(1 + \tilde{\gamma}_v)}}{2\tilde{D}_v - Pe^2} \right]^{1/2} = 10^{-3} > t'_{III}$ . We list the dominance of different kinds of fluctuations in different time regimes in table 1.

**Table 1.**  $\langle \mathbf{r}^2 \rangle$  scaling: characterizing dominance of fluctuation in different regime  
Direction of increasing time  $t \longrightarrow$

$\langle \mathbf{r}^2 \rangle$	$\sim t$	$\sim t^2$	$\sim t$	$\sim t^2$	$\sim t$
$(d-1)D_r \gg \gamma_v$	thermal	orientation	thermal + orientation	speed	thermal + orientation + speed
$(d-1)D_r \ll \gamma_v$	thermal	speed	thermal + speed	orientation	thermal + speed + orientation

## 6.2. Displacement fluctuations

In this Section, we compute the displacement fluctuation  $\langle \delta \mathbf{r}^2 \rangle$  and analyze the multiple crossovers that it shows identifying the crossover times. The displacement fluctuation is defined as  $\langle \delta \mathbf{r}^2 \rangle = \langle \mathbf{r}^2 \rangle - \langle \mathbf{r} \rangle^2$  where  $\langle \mathbf{r}^2 \rangle$  and  $\langle \mathbf{r} \rangle$  were already calculated in equations (21) and (15). Thus, in  $d$ -dimensions,

$$\begin{aligned} \langle \delta \mathbf{r}^2 \rangle = & 2d \left( D + \frac{v_0^2}{(d-1)dD_r} \right) t - \frac{v_0^2}{(d-1)^2 D_r^2} (3 - 4e^{-(d-1)D_r t} + e^{-2(d-1)D_r t}) \\ & + \frac{2D_v}{\gamma_v(\gamma_v + (d-1)D_r)} \left[ t - \frac{1 - e^{-(\gamma_v + (d-1)D_r)t}}{(\gamma_v + (d-1)D_r)} - \frac{1 - e^{-2\gamma_v t}}{2\gamma_v} + \frac{e^{-2\gamma_v t} - e^{-(\gamma_v + (d-1)D_r)t}}{((d-1)D_r - \gamma_v)} \right]. \end{aligned} \quad (29)$$

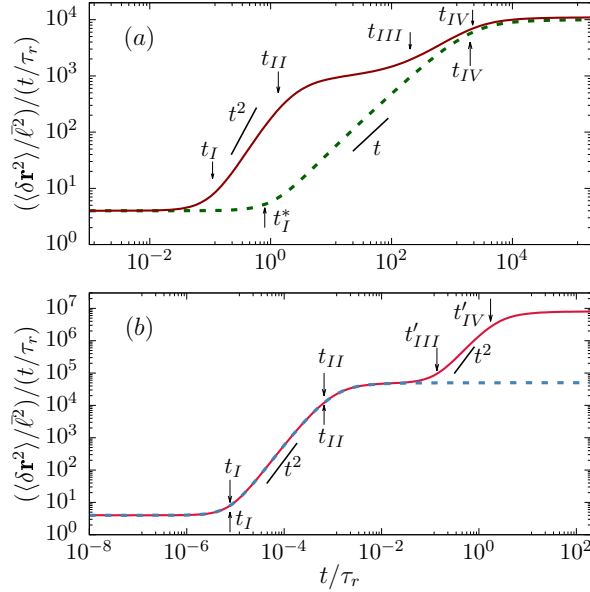


**Figure 4.** (color online) Displacement fluctuations  $\langle \delta \mathbf{r}^2 \rangle$  in equation (29) as a function of time  $t$  using  $d = 2$ . (a) Parameters used are  $\tilde{\gamma}_v = 5 \times 10^{-4}$ ,  $\tilde{D}_v = 2.5$  with active speed  $Pe = 22.36$  (solid line), 1.12 (dashed line). The solid line shows four crossovers with crossover times  $t_I/\tau_r = 0.008$ ,  $t_{II}/\tau_r = 3.03$ ,  $t_{III}/\tau_r = 202.8$  and  $t_{IV}/\tau_r = 2.2 \times 10^3$ . The dashed line shows two crossovers with crossover times  $t_I^*/\tau_r = 0.8$  and  $t_{IV}/\tau_r = 2 \times 10^3$ . (b) Parameters used are  $\tilde{\gamma}_v = 2 \times 10^3$ ,  $\tilde{D}_v = 10^{11}$  with  $Pe = 2 \times 10^3$  (solid line), 10 (dashed line). The solid line exhibits four crossovers with crossover times  $t_I/\tau_r = 8 \times 10^{-6}$ ,  $t_{II}/\tau_r = 7 \times 10^{-4}$ ,  $t'_{III}/\tau_r = 1.4 \times 10^{-1}$  and  $t'_{IV}/\tau_r = 1.7$ . The dashed line shows two crossovers with crossover times  $t_I/\tau_r = 8 \times 10^{-6}$ ,  $t_{II}/\tau_r = 7 \times 10^{-4}$ .

In the small time limit of  $D_r t \ll 1$ ,  $\gamma_v t \ll 1$ , expanding  $\langle \delta \mathbf{r}^2 \rangle$  in equation (29) around  $t = 0$  leads to,

$$\langle \delta \mathbf{r}^2 \rangle = 2dDt + \frac{2}{3}(D_v + (d-1)D_r v_0^2)t^3 - \frac{1}{6}[(d-1)D_r D_v + 3D_v \gamma_v + 3(d-1)^2 D_r^2 v_0^2]t^4 + \mathcal{O}(t^5). \quad (30)$$

The first two terms in the expansion shows a possible crossover from  $\langle \delta \mathbf{r}^2 \rangle \sim t$  to  $\sim t^3$  at  $t_I = [3dD/(D_v + (d-1)D_r v_0^2)]^{1/2}$ . Moreover, a second crossover from  $\langle \delta \mathbf{r}^2 \rangle \sim t^3$  to  $\sim t$  can appear at  $t_{II} = 4(D_v + (d-1)D_r v_0^2)/((d-1)D_r D_v + 3D_v \gamma_v + 3v_0^2(d-1)^2 D_r^2)$ . In the long time limit of  $t \rightarrow \infty$ , i.e.,  $D_r t \gg 1$ ,  $\gamma_v t \gg 1$ ,  $\langle \delta \mathbf{r}^2 \rangle$  in equation (29) leads to a diffusive behavior

$$\langle \delta \mathbf{r}^2 \rangle = \left( 2dD + \frac{2v_0^2}{(d-1)D_r} + \frac{2D_v}{\gamma_v(\gamma_v + (d-1)D_r)} \right) t. \quad (31)$$

(i) **Slow relaxation of active speed;**  $\gamma_v \ll (d-1)D_r$  : In the limit of  $(d-1)D_r t \gg 1$  and  $2\gamma_v t \ll 1$ ,  $\langle \delta \mathbf{r}^2 \rangle$  in equation (29) leads to

$$\langle \delta \mathbf{r}^2 \rangle = \left( 2dD + \frac{2v_0^2}{(d-1)D_r} + \frac{4D_v}{((d-1)^2 D_r^2 - \gamma_v^2)} \right) t + \frac{2D_v}{((d-1)D_r - \gamma_v)} t^2 + \mathcal{O}(t^3). \quad (32)$$

This allows a third crossover from  $\langle \delta \mathbf{r}^2 \rangle \sim t$  to  $\langle \delta \mathbf{r}^2 \rangle \sim t^2$  at  $t_{III} \sim (2dD + 2v_0^2/(d-1)D_r + 4D_v/((d-1)^2 D_r^2 - \gamma_v^2))/((d-1)D_r - \gamma_v)/2D_v$ . Finally, a crossover from  $\langle \delta \mathbf{r}^2 \rangle \sim t^2$  to  $\sim t$  can appear at  $t_{IV} \sim [2dD + 2v_0^2/(d-1)D_r + 2D_v/\{\gamma_v(\gamma_v + (d-1)D_r)\}]/((d-1)D_r - \gamma_v)/2D_v$ .

In the case of  $t_{II} < t_I$ , the number of possible crossovers reduces to two: from  $\langle \delta \mathbf{r}^2 \rangle \sim t$  to  $\sim t^2$  to  $\sim t$ . Following a procedure similar to the analysis of crossovers in  $\langle \mathbf{r}^2 \rangle$ , we find that the first crossover from  $\langle \delta \mathbf{r}^2 \rangle \sim t$  to  $\sim t^2$  appears at  $t_I^* \sim 2dD((d-1)D_r - \gamma_v)/2D_v$ , obtained by comparing the first term in equation (30) and the second term in equation (32). The second crossover  $\langle \delta \mathbf{r}^2 \rangle \sim t^2$  to  $\sim t$  appears at  $t_{IV} \sim [2dD + 2v_0^2/(d-1)D_r + 2D_v/\{\gamma_v(\gamma_v + (d-1)D_r)\}]/((d-1)D_r - \gamma_v)/2D_v$ , obtained by comparing the second terms in equation (32) and equation (31).

In figure 4(a) we show two examples of crossovers in  $\langle \delta \mathbf{r}^2 \rangle$  observed in 2d in the limit of  $\gamma_v \tau_r \ll 1$ . We identify the crossover times in the figure. The figure is for parameter values  $\tilde{\gamma}_v = \gamma_v \tau_r = 5 \times 10^{-4}$ ,  $\tilde{D}_v = D_v \tau_r / \bar{v}^2 = 2.5$ . The solid line,  $Pe = v_0 / \bar{v} = 22.36$  in figure 4(a) exhibits all the four crossovers  $\langle \delta \mathbf{r}^2 \rangle \sim t$  to  $\sim t^3$ , to  $\sim t$ , to  $\sim t^2$ , to finally  $\sim t$  as the requirement  $t_I < t_{II} < t_{III} < t_{IV}$  is satisfied. The crossover times are  $t_I/\tau_r \sim [6/(Pe^2 + \tilde{D}_v)]^{1/2} \approx 0.11$ ,  $t_{II}/\tau_r \sim 4(Pe^2 + \tilde{D}_v)/(3Pe^2 + 3\tilde{D}_v\tilde{\gamma}_v + \tilde{D}_v) \approx 1.34$ ,  $t_{III}/\tau_r \sim [4 + 2Pe^2 + 4\tilde{D}_v/(1 - \tilde{\gamma}_v^2)](1 - \tilde{\gamma}_v)/2\tilde{D}_v \approx 202.8$  and  $t_{IV}/\tau_r \sim [4 + 2Pe^2 + 2\tilde{D}_v/\{\tilde{\gamma}_v(1 + \tilde{\gamma}_v)\}]/(1 - \tilde{\gamma}_v)/2\tilde{D}_v \approx 2200$ . The dashed line for  $Pe = v_0 / \bar{v} = 1.12$  in figure 4(a) shows two crossovers  $\langle \delta \mathbf{r}^2 \rangle \sim t$  to  $\sim t^2$  to  $\sim t$  as  $t_{II} < t_I$ . The crossover times are  $t_I^*/\tau_r \sim 2(1 - \tilde{\gamma}_v)/\tilde{D}_v \approx 0.8$  and  $t_{IV}/\tau_r \approx 2 \times 10^3$ . Here, the first diffusive-ballistic crossover appears at  $t_I^*$  as  $t_I^* < t_I \approx 1.3 \tau_r$ .

(ii) **Fast relaxation of active speed;**  $\gamma_v \gg (d-1)D_r$  : In the other limit of  $(d-1)D_r t \ll 1$  and  $2\gamma_v t \gg 1$ , using  $\exp(-2\gamma_v t) = 0$ ,  $\exp[-((d-1)D_r + \gamma_v)t] = 0$  and expanding  $\exp(-D_r t)$  around  $D_r t = 0$ , equation (29) leads to

$$\langle \delta \mathbf{r}^2 \rangle \simeq \left( 2dD + \frac{2D_v}{\gamma_v((d-1)D_r + \gamma_v)} \right) t + \frac{2}{3}(d-1)D_r v_0^2 t^3. \quad (33)$$

This predicts a third possible crossover from  $\langle \delta \mathbf{r}^2 \rangle \sim t$  to  $\sim t^3$  at  $t'_{III} \sim [3(dD + D_v/\{\gamma_v((d-1)D_r + \gamma_v)\})/(d-1)D_r v_0^2]^{1/2}$ . The final crossover  $\langle \delta \mathbf{r}^2 \rangle \sim t^3$  to  $\sim t$  can appear at  $t'_{IV} \sim [3(dD + v_0^2/(d-1)D_r + D_v/\{\gamma_v((d-1)D_r + \gamma_v)\})/(d-1)D_r v_0^2]^{1/2}$ , with the crossover point obtained by comparing the second term in equation (33) with equation (31). If  $t'_{IV} \leq t'_{III}$  these last two crossovers will not be possible.

We demonstrate such crossovers in 2d, in the limit of  $\gamma_v \tau_r \gg 1$ , in figure 4(b). The parameter values used are  $\tilde{\gamma}_v = \gamma_v \tau_r = 2 \times 10^3$ ,  $\tilde{D}_v = D_v \tau_r / \bar{v}^2 = 10^{11}$ . The solid line in figure 4(b) depicts the behavior at  $Pe = v_0 / \bar{v} = 2 \times 10^3$ . This exhibits all four crossovers from  $\langle \mathbf{r}^2 \rangle \sim t$  to  $\langle \mathbf{r}^2 \rangle \sim t^3$  to  $\langle \mathbf{r}^2 \rangle \sim t$  to  $\langle \mathbf{r}^2 \rangle \sim t^3$  to finally  $\langle \mathbf{r}^2 \rangle \sim t$  as the requirement  $t_I < t_{II} < t_{III} < t_{IV}$  is satisfied. In this case, the crossover points  $t_I/\tau_r \sim [6/(\tilde{D}_v + Pe^2)]^{1/2} \approx 8 \times 10^{-6}$ ,  $t_{II}/\tau_r \sim 4(\tilde{D}_v + Pe^2)/[\tilde{D}_v + 3\tilde{D}_v\tilde{\gamma}_v + 3Pe^2] \approx 7 \times 10^{-4}$ ,  $t'_{III}/\tau_r \sim [3[2 + \tilde{D}_v/\{\tilde{\gamma}_v(1 + \tilde{\gamma}_v)\}]/Pe^2]^{1/2} \approx 1.4 \times 10^{-1}$ , and  $t'_{IV}/\tau_r \sim [3(2 + Pe^2 + \tilde{D}_v/\{\tilde{\gamma}_v(1 + \tilde{\gamma}_v)\})/Pe^2]^{1/2} \approx 1.7$  are identified in figure 4(b). The dashed line corresponding to  $Pe = v_0 / \bar{v} = 10$  in figure 4(b) shows two crossovers from  $\langle \delta \mathbf{r}^2 \rangle \sim t$ ,

to  $\langle \delta \mathbf{r}^2 \rangle \sim t^3$  to finally  $\langle \delta \mathbf{r}^2 \rangle \sim t$ . As  $t'_{III} \approx t'_{IV} \approx 27.4 \tau_r$ , the corresponding crossovers from  $\langle \delta \mathbf{r}^2 \rangle \sim t$  to  $\sim t^3$  to  $\sim t$  is absent. The crossover times are  $t_I/\tau_r \sim \left[6/(\tilde{D}_v + Pe^2)\right]^{1/2} \approx 8 \times 10^{-6}$  and  $t_{II}/\tau_r \sim 4(\tilde{D}_v + Pe^2)/(\tilde{D}_v + 3\tilde{D}_v\tilde{\gamma}_v + 3Pe^2) \approx 7 \times 10^{-4}$ .

### 6.3. Components of displacement fluctuation

The displacement of the ABP in parallel and perpendicular directions with respect to the initial heading direction  $\hat{\mathbf{u}}_0$  is studied here to identify any possible anisotropy in the dynamics. The mean displacements are  $\langle r_{\parallel} \rangle = \langle \mathbf{r} \rangle \cdot \hat{\mathbf{u}}_0 \neq 0$  and  $\langle \mathbf{r}_{\perp} \rangle = \langle \mathbf{r} \rangle - \langle r_{\parallel} \rangle \hat{\mathbf{u}}_0$ . Here  $\langle \mathbf{r}_{\perp} \rangle = 0$  in the absence of external drive. In this Section, we compute the parallel and normal components of mean-squared displacements and displacement fluctuations.

*6.3.1. Parallel component:* We consider the initial active speed  $v_1 = v_0$ . Without any loss of generality, let us assume the initial heading direction of activity is towards the  $x$ -axis,  $\hat{\mathbf{u}}_0 = \hat{x}$ . We use equation (5). Here  $\psi = r_{\parallel}^2 = x^2$ , giving  $\langle \psi \rangle_0 = 0$ ,  $\langle \nabla_r^2 \psi \rangle_s = 2\langle 1 \rangle_s$ ,  $\langle \nabla_u^2 \psi \rangle_s = 0$ ,  $\langle \partial_v^2 \psi \rangle_s = 0$ ,  $\langle (v - v_0) \partial_v \psi \rangle_s = 0$ , and  $\langle v \hat{\mathbf{u}} \cdot \nabla \psi \rangle_s = 2\langle v x u_x \rangle_s$ . Thus we find

$$\langle r_{\parallel}^2 \rangle_s = \frac{1}{s} [2D\langle 1 \rangle_s + 2\langle v x u_x \rangle_s].$$

To proceed we consider  $\psi = v x u_x$ , giving  $\langle \psi \rangle_0 = 0$ ,  $\langle \nabla_r^2 \psi \rangle_s = 0$ ,  $\langle \nabla_u^2 \psi \rangle_s = -(d-1)\langle v x u_x \rangle_s$ , and  $\langle \hat{\mathbf{u}} \cdot \nabla \psi \rangle_s = \langle v u_x^2 \rangle_s$ , leading to  $\langle v x u_x \rangle_s = [\langle v^2 u_x^2 \rangle_s + \gamma_v v_0 \langle x u_x \rangle_s] / (s + (d-1)D_r + \gamma_v)$ . Further,  $\langle x u_x \rangle_s = \langle v u_x^2 \rangle_s / (s + (d-1)D_r)$ . Further, we find,  $\langle v u_x^2 \rangle_s = \frac{v_0(s+2D_r)}{s(s+2dD_r)}$  and

$$\langle v^2 u_x^2 \rangle_s = \frac{v_0^2(s+2D_r)}{s(s+2dD_r)} + \frac{4D_r D_v}{s(s+2\gamma_v)(s+2dD_r)} + \frac{2D_v(s+2\gamma_v+2D_r)}{(s+2\gamma_v)(s+2dD_r)(s+2\gamma_v+2dD_r)}.$$

Thus using these relations, we obtain

$$\begin{aligned} \langle r_{\parallel}^2 \rangle_s &= \frac{2D}{s^2} + \frac{2v_0^2(s+2D_r)}{s^2(s+(d-1)D_r)(s+2dD_r)} + \frac{8D_r D_v}{s^2(s+2\gamma_v)(s+2dD_r)(s+\gamma_v+(d-1)D_r)} \\ &+ \frac{4D_v(s+2\gamma_v+2D_r)}{s(s+2\gamma_v)(s+2dD_r)(s+2\gamma_v+2dD_r)(s+\gamma_v+(d-1)D_r)}. \end{aligned} \quad (34)$$

The inverse Laplace transform gives,

$$\begin{aligned} \langle r_{\parallel}^2 \rangle &= 2 \left( D + \frac{v_0^2}{(d-1)dD_r} \right) t \\ &+ \frac{v_0^2}{D_r^2} \left( \frac{(d-1)e^{-2dD_r t}}{d^2(d+1)} + \frac{2(3-d)e^{-(d-1)D_r t}}{(d-1)^2(d+1)} + \frac{d^2-4d+1}{(d-1)^2 d^2} \right) \\ &+ 8D_r D_v \left[ \frac{-d^2 D_r^2 - 4d\gamma_v D_r + dD_r^2 - \gamma_v^2 + \gamma_v D_r}{8d^2 \gamma_v^2 D_r^2 ((d-1)D_r + \gamma_v)^2} + \frac{t}{4d\gamma_v D_r ((d-1)D_r + \gamma_v)} \right] \\ &+ \frac{8D_r D_v e^{-2dD_r t}}{8d^2 D_r^2 (dD_r - \gamma_v)((d+1)D_r - \gamma_v)} \\ &- 8D_r D_v \frac{e^{-((d-1)D_r + \gamma_v)t}}{((d+1)D_r - \gamma_v)((d-1)D_r - \gamma_v)((d-1)D_r + \gamma_v)^2} \end{aligned}$$

$$\begin{aligned}
& +8D_r D_v \frac{e^{-2\gamma_v t}}{8\gamma_v^2(dD_r - \gamma_v)((d-1)D_r - \gamma_v)} + 4D_v \frac{((d-1)D_r - \gamma_v)e^{-2dD_r t}}{4d\gamma_v D_r(dD_r - \gamma_v)((d+1)D_r - \gamma_v)} \\
& +4D_v \left[ \frac{D_r + \gamma_v}{4d\gamma_v D_r(dD_r + \gamma_v)((d-1)D_r + \gamma_v)} - \frac{(d-1)e^{-(2dD_r + 2\gamma_v)t}}{4d\gamma_v(dD_r + \gamma_v)((d+1)D_r + \gamma_v)} \right] \\
& +4D_v \left[ \frac{((3-d)D_r + \gamma_v)e^{-((d-1)D_r + \gamma_v)t}}{((d+1)^2 D_r^2 - \gamma_v^2)((d-1)^2 D_r^2 - \gamma_v^2)} - \frac{e^{-2\gamma_v t}}{4d\gamma_v(dD_r - \gamma_v)((d-1)D_r - \gamma_v)} \right].
\end{aligned} \tag{35}$$

Thus the parallel component of the displacement fluctuation  $\langle \delta r_{\parallel}^2 \rangle = \langle r_{\parallel}^2 \rangle - \langle r_{\parallel} \rangle^2$  is given by,

$$\begin{aligned}
\langle \delta r_{\parallel}^2 \rangle & = 2 \left( D + \frac{v_0^2}{(d-1)dD_r} \right) t \\
& + \frac{v_0^2}{D_r^2} \left( \frac{(d-1)e^{-2dD_r t}}{d^2(d+1)} + \frac{8e^{-(d-1)D_r t}}{(d-1)^2(d+1)} - \frac{e^{-2(d-1)D_r t}}{(d-1)^2} - \frac{4d-1}{(d-1)^2 d^2} \right) \\
& + 8D_r D_v \left[ \frac{-d^2 D_r^2 - 4d\gamma_v D_r + dD_r^2 - \gamma_v^2 + \gamma_v D_r}{8d^2 \gamma_v^2 D_r^2 ((d-1)D_r + \gamma_v)} + \frac{t}{4d\gamma_v D_r ((d-1)D_r + \gamma_v)} \right] \\
& + \frac{8D_r D_v e^{-2dD_r t}}{8d^2 D_r^2 (dD_r - \gamma_v)((d+1)D_r - \gamma_v)} \\
& - 8D_r D_v \frac{e^{-((d-1)D_r + \gamma_v)t}}{((d+1)D_r - \gamma_v)((d-1)D_r - \gamma_v)((d-1)D_r + \gamma_v)^2} \\
& + 8D_r D_v \frac{e^{-2\gamma_v t}}{8\gamma_v^2(dD_r - \gamma_v)((d-1)D_r - \gamma_v)} + 4D_v \frac{((d-1)D_r - \gamma_v)e^{-2dD_r t}}{4d\gamma_v D_r(dD_r - \gamma_v)((d+1)D_r - \gamma_v)} \\
& + 4D_v \left[ \frac{D_r + \gamma_v}{4d\gamma_v D_r(dD_r + \gamma_v)((d-1)D_r + \gamma_v)} - \frac{(d-1)e^{-(2dD_r + 2\gamma_v)t}}{4d\gamma_v(dD_r + \gamma_v)((d+1)D_r + \gamma_v)} \right] \\
& + 4D_v \left[ \frac{((3-d)D_r + \gamma_v)e^{-((d-1)D_r + \gamma_v)t}}{((d+1)^2 D_r^2 - \gamma_v^2)((d-1)^2 D_r^2 - \gamma_v^2)} - \frac{e^{-2\gamma_v t}}{4d\gamma_v(dD_r - \gamma_v)((d-1)D_r - \gamma_v)} \right].
\end{aligned} \tag{36}$$

*6.3.2. Perpendicular component:* The fluctuations in the perpendicular component

$$\begin{aligned}
\langle \delta \mathbf{r}_{\perp}^2 \rangle & = \langle \delta \mathbf{r}^2 \rangle - \langle \delta r_{\parallel}^2 \rangle = 2(d-1) \left( D + \frac{v_0^2}{(d-1)dD_r} \right) t \\
& + \frac{v_0^2}{D_r^2} \left( \frac{4e^{-(d-1)D_r t}}{d^2 - 1} - \frac{(d-1)e^{-2dD_r t}}{d^2(d+1)} - \frac{3d-1}{d^2(d-1)} \right) \\
& + \frac{2D_v}{\gamma_v(\gamma_v + (d-1)D_r)} \left[ t - \frac{1 - e^{-(\gamma_v + (d-1)D_r)t}}{(\gamma_v + (d-1)D_r)} - \frac{1 - e^{-2\gamma_v t}}{2\gamma_v} + \frac{e^{-2\gamma_v t} - e^{-(d-1)D_r t}}{((d-1)D_r - \gamma_v)} \right] \\
& - 8D_r D_v \left[ \frac{-d^2 D_r^2 - 4d\gamma_v D_r + dD_r^2 - \gamma_v^2 + \gamma_v D_r}{8d^2 \gamma_v^2 D_r^2 ((d-1)D_r + \gamma_v)} + \frac{t}{4d\gamma_v D_r ((d-1)D_r + \gamma_v)} \right] \\
& - \frac{8D_r D_v e^{-2dD_r t}}{8d^2 D_r^2 (dD_r - \gamma_v)((d+1)D_r - \gamma_v)} \\
& + 8D_r D_v \frac{e^{-((d-1)D_r + \gamma_v)t}}{((d+1)D_r - \gamma_v)((d-1)D_r - \gamma_v)((d-1)D_r + \gamma_v)^2}
\end{aligned}$$

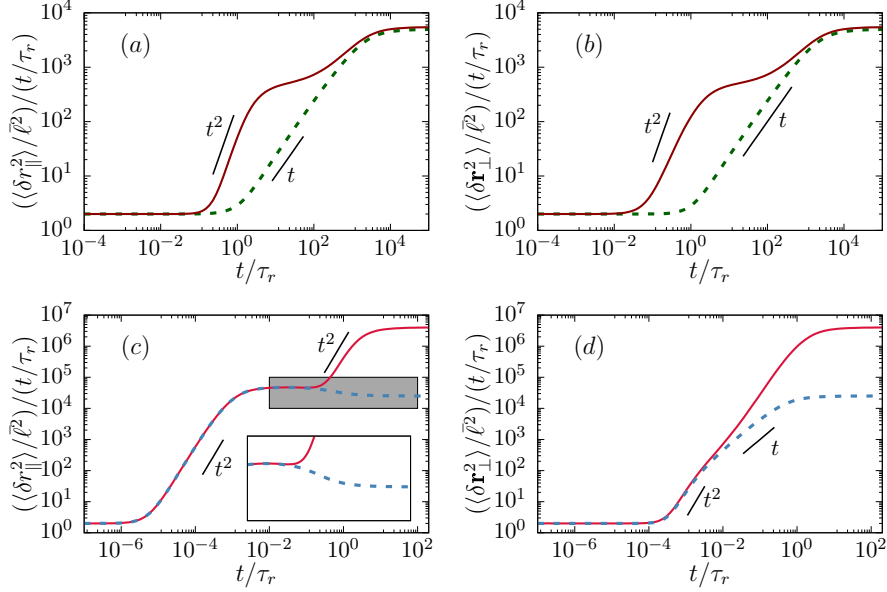


**Figure 5.** (color online) Components of displacement fluctuation, (a, c)  $\langle \delta r_{\parallel}^2 \rangle$  and (b, d)  $\langle \delta r_{\perp}^2 \rangle$  as a function of time  $t$  in 2d. (a, b)  $\tilde{\gamma}_v = 5 \times 10^{-4}$ ,  $\tilde{D}_v = 2.5$  with  $Pe = 22.36$  (solid line), 1.12 (dashed line). (c, d)  $\tilde{\gamma}_v = 2 \times 10^3$ ,  $\tilde{D}_v = 10^{11}$  with  $Pe = 2 \times 10^3$  (solid line), 10 (dashed line). The inset in Figure (c) displaying a zoomed in view of the shaded region in the main figure shows a sub-diffusive behavior in the parallel component of displacement fluctuation over an intermediate time regime.

$$\begin{aligned}
& -8D_r D_v \frac{e^{-2\gamma_v t}}{8\gamma_v^2 (dD_r - \gamma_v)((d-1)D_r - \gamma_v)} - 4D_v \frac{((d-1)D_r - \gamma_v)e^{-2dD_r t}}{4d\gamma_v D_r (dD_r - \gamma_v)((d+1)D_r - \gamma_v)} \\
& -4D_v \left[ \frac{D_r + \gamma_v}{4d\gamma_v D_r (dD_r + \gamma_v)((d-1)D_r + \gamma_v)} - \frac{(d-1)e^{-(2dD_r + 2\gamma_v)t}}{4d\gamma_v (dD_r + \gamma_v)((d+1)D_r + \gamma_v)} \right] \\
& -4D_v \left[ \frac{((3-d)D_r + \gamma_v)e^{-((d-1)D_r + \gamma_v)t}}{((d+1)^2 D_r^2 - \gamma_v^2)((d-1)^2 D_r^2 - \gamma_v^2)} - \frac{e^{-2\gamma_v t}}{4d\gamma_v (dD_r - \gamma_v)((d-1)D_r - \gamma_v)} \right].
\end{aligned} \tag{37}$$

In figure 5 we show various possible features of  $\langle \delta r_{\parallel}^2 \rangle$  and  $\langle \delta r_{\perp}^2 \rangle$  at different parameter regimes. ABPs without speed fluctuations display anisotropy in displacement fluctuations, with  $\langle \delta r_{\parallel}^2 \rangle$  showing a crossover from  $\sim t$  to  $\sim t^4$ , in contrast to the  $\sim t$  to  $\sim t^3$  crossover found in  $\langle \delta r_{\perp}^2 \rangle$  [21]. Similar asymmetry in the absence of thermal fluctuations was pointed out before in Ref. [17]. As is shown in figure 5(a) and (b), such a clear distinction in the components of displacement fluctuation can disappear in the presence of speed fluctuations. Depending on the  $Pe$  value, both  $\langle \delta r_{\parallel}^2 \rangle$  and  $\langle \delta r_{\perp}^2 \rangle$  can show  $\sim t$  to  $\sim t^2$  to  $\sim t$  crossovers, or,  $\sim t$  to  $\sim t^3$  to  $\sim t$  to  $\sim t^2$  to  $\sim t$  crossovers. However, in the presence of large speed fluctuations and at larger  $Pe$  the parallel component  $\langle \delta r_{\parallel}^2 \rangle$  can even display sub-diffusive behavior in intermediate times (figure 5(c)). This is qualitatively different from crossovers shown by  $\langle \delta r_{\perp}^2 \rangle$  as is demonstrated in figure 5(d).

The identification of multiple crossovers in the mean-squared displacement, displacement fluctuations, and its components is the second main result of this paper.

## 7. Fourth moment and kurtosis

In this Section, we present exact calculations for the fourth moments of active speed and displacement. The fourth moment of speed calculated from the Fokker-Planck equation is consistent with the underlying Gaussian process. The analytic predictions for the fourth moment of displacement shows agreement with direct numerical simulations. We further compute the kurtosis of displacement vector to capture the deviations from the Gaussian fluctuations. For these calculations we consider the initial active speed of the particle to be  $v_1 = Pe\bar{v}$  and the initial position at the origin.

### 7.1. Fourth moment of speed

Using  $\psi = v^4$  in equation (5), we get,  $\langle v^4 \rangle_s = [v_0^4 + 12D_v \langle v^2 \rangle_s + 4\gamma_v v_0 \langle v^3 \rangle_s] / (s + 4\gamma_v)$  where,  $\langle v^2 \rangle_s = v_0^2/s + 2D_v/s(s + 2\gamma_v)$ ,  $\langle v^3 \rangle_s = v_0^3/s + 6D_v v_0/s(s + 2\gamma_v)$ . This leads to,

$$\langle v^4 \rangle_s = \frac{v_0^4}{s} + \frac{12D_v v_0^2}{s(s + 2\gamma_v)} + \frac{24D_v^2}{s(s + 2\gamma_v)(s + 4\gamma_v)}.$$

Performing inverse Laplace transform we find

$$\langle v^4 \rangle = v_0^4 + \frac{6D_v(\gamma_v v_0^2 + D_v)}{\gamma_v^2} (1 - e^{-2\gamma_v t}) - \frac{3D_v^2}{\gamma_v^2} (1 - e^{-4\gamma_v t}).$$

Writing  $v = \delta v + \langle v \rangle$ , Wick's theorem for a Gaussian process predicts  $\langle v^4 \rangle = \langle v \rangle^4 + 6\langle v \rangle^2 \langle \delta v^2 \rangle + 3\langle \delta v^2 \rangle^2$ . The above expression agrees with this behavior.

### 7.2. Fourth moment of displacement

Using  $\psi = \mathbf{r}^4$  in equation (5), we get

$$\langle \mathbf{r}^4 \rangle_s = \frac{1}{s} [4(d + 2)D \langle \mathbf{r}^2 \rangle_s + 4\langle v(\hat{\mathbf{u}} \cdot \mathbf{r}) \mathbf{r}^2 \rangle_s], \quad (38)$$

where  $\langle \mathbf{r}^2 \rangle_s$  has been already calculated in equation(19). Similarly, using equation (5) we can calculate the various moments necessary to evaluate  $\langle \mathbf{r}^4 \rangle_s$ . We list them below,

$$\langle v(\hat{\mathbf{u}} \cdot \mathbf{r}) \mathbf{r}^2 \rangle_s = \frac{2(2 + d)D \langle v \hat{\mathbf{u}} \cdot \mathbf{r} \rangle_s + \langle v^2 \mathbf{r}^2 \rangle_s + 2\langle v^2 (\hat{\mathbf{u}} \cdot \mathbf{r})^2 \rangle_s + \gamma_v v_0 \langle (\hat{\mathbf{u}} \cdot \mathbf{r}) \mathbf{r}^2 \rangle_s}{s + (d - 1)D_r + \gamma_v},$$

$$\langle v \hat{\mathbf{u}} \cdot \mathbf{r} \rangle_s = \frac{\langle v^2 \rangle_s + \gamma_v v_0 \langle \hat{\mathbf{u}} \cdot \mathbf{r} \rangle_s}{s + (d - 1)D_r + \gamma_v},$$

$$\langle v^2 \mathbf{r}^2 \rangle_s = \frac{2dD \langle v^2 \rangle_s + 2\langle v^3 \hat{\mathbf{u}} \cdot \mathbf{r} \rangle_s + 2D_v \langle \mathbf{r}^2 \rangle_s + 2\gamma_v v_0 \langle v \mathbf{r}^2 \rangle_s}{s + 2\gamma_v},$$

$$\langle v^2 (\hat{\mathbf{u}} \cdot \mathbf{r})^2 \rangle_s = \frac{2D \langle v^2 \rangle_s + 2D_r \langle v^2 \mathbf{r}^2 \rangle_s + 2D_v \langle (\hat{\mathbf{u}} \cdot \mathbf{r})^2 \rangle_s + 2\langle v^3 \hat{\mathbf{u}} \cdot \mathbf{r} \rangle_s + 2\gamma_v v_0 \langle v (\hat{\mathbf{u}} \cdot \mathbf{r})^2 \rangle_s}{s + 2dD_r + 2\gamma_v},$$

$$\langle (\hat{\mathbf{u}} \cdot \mathbf{r}) \mathbf{r}^2 \rangle_s = \frac{2(2 + d)D \langle \hat{\mathbf{u}} \cdot \mathbf{r} \rangle_s + \langle v \mathbf{r}^2 \rangle_s + 2\langle v (\hat{\mathbf{u}} \cdot \mathbf{r})^2 \rangle_s}{s + (d - 1)D_r},$$

The calculations of these terms, in turn, require the following results,

$$\begin{aligned}
\langle v^2 \rangle_s &= \frac{v_0^2}{s} + \frac{2D_v}{s(s+2\gamma_v)}, \quad \langle v^3 \rangle_s = \frac{v_0^3}{s} + \frac{6D_v v_0}{s(s+2\gamma_v)}, \\
\langle \hat{\mathbf{u}} \cdot \mathbf{r} \rangle_s &= \frac{v_0}{s(s+(d-1)D_r)}, \quad \langle (\hat{\mathbf{u}} \cdot \mathbf{r})^2 \rangle_s = \frac{2D\langle 1 \rangle_s + 2D_r \langle \mathbf{r}^2 \rangle_s + 2\langle v \hat{\mathbf{u}} \cdot \mathbf{r} \rangle_s}{s+2dD_r}, \\
\langle v^2 \hat{\mathbf{u}} \cdot \mathbf{r} \rangle_s &= \frac{2D_v \langle \hat{\mathbf{u}} \cdot \mathbf{r} \rangle_s + \langle v^3 \rangle_s + 2\gamma_v v_0 \langle v \hat{\mathbf{u}} \cdot \mathbf{r} \rangle_s}{s+(d-1)D_r+2\gamma_v}, \\
\langle v^3 \hat{\mathbf{u}} \cdot \mathbf{r} \rangle_s &= \frac{6D_v \langle v \langle \hat{\mathbf{u}} \cdot \mathbf{r} \rangle_s + \langle v^4 \rangle_s + 3\gamma_v v_0 \langle v^2 \hat{\mathbf{u}} \cdot \mathbf{r} \rangle_s}{s+(d-1)D_r+3\gamma_v}, \\
\langle v \mathbf{r}^2 \rangle_s &= \frac{2dD\langle v \rangle_s + 2\langle v^2 \hat{\mathbf{u}} \cdot \mathbf{r} \rangle_s + \gamma_v v_0 \langle \mathbf{r}^2 \rangle_s}{s+\gamma_v}, \\
\langle v (\hat{\mathbf{u}} \cdot \mathbf{r})^2 \rangle_s &= \frac{2D\langle v \rangle_s + 2D_r \langle v \mathbf{r}^2 \rangle_s + 2\langle v^2 \hat{\mathbf{u}} \cdot \mathbf{r} \rangle_s + \gamma_v v_0 \langle (\hat{\mathbf{u}} \cdot \mathbf{r})^2 \rangle_s}{s+2dD_r+\gamma_v},
\end{aligned}$$

Finally, performing inverse Laplace transform of equation(38) one obtains the expression for  $\langle \mathbf{r}^4 \rangle(t)$ . The expression is too lengthy to show here. Instead, we plot the expression for  $\langle \mathbf{r}^4 \rangle$  as a function of time in figure 6. In the following, we present the short and long time limit of  $\langle \mathbf{r}^4 \rangle(t)$ , and analyze its behavior. In the short time limit, an expansion of  $\langle \mathbf{r}^4 \rangle$  around  $t = 0$  gives,

$$\langle \mathbf{r}^4 \rangle = 4d(d+2)D^2 t^2 + 4(d+2)Dv_0^2 t^3 + \left( v_0^4 - \frac{4(d+2)D}{3} ((d-1)D_r v_0^2 - 2D_v) \right) t^4 + \mathcal{O}(t^5). \quad (39)$$

It shows that a  $\langle \mathbf{r}^4 \rangle \sim t^2$  scaling at shortest time, which crosses over to  $\langle \mathbf{r}^4 \rangle(t) \sim t^3$  scaling at  $t_I = dD/v_0^2$ . The crossover point is obtained by comparing the first two terms in the above expansion. A comparison between the second and third terms of the above expansion shows that a second crossover from  $\langle \mathbf{r}^4 \rangle \sim t^3$  to  $\sim t^4$  can appear at,

$$t_{II} = \frac{12(d+2)Dv_0^2}{3v_0^4 - 4(d+2)D((d-1)D_r v_0^2 - 2D_v)},$$

provided  $t_{II} > t_I$ . In the long time limit,  $\langle \mathbf{r}^4 \rangle$  approaches,

$$\langle \mathbf{r}^4 \rangle \approx \frac{4(2+d)[(d-1)D_r(D_v + dD\gamma_v((d-1)D_r + \gamma_v)) + \gamma_v((d-1)D_r + \gamma_v)v_0^2]^2}{d(d-1)^2 D_r^2 \gamma_v^2 ((d-1)D_r + \gamma_v)^2} t^2.$$

In figure 6(a,b), we show comparisons between the analytic expression for  $\langle \mathbf{r}^4 \rangle$  and the direct numerical simulation result for this fourth moment to find clear agreement between them. Figure 6(a) corresponds to the limit  $D_r \ll \gamma_v$  and figure 6(b) is plotted for parameter values obeying  $D_r \gg \gamma_v$ .

### 7.3. Kurtosis: deviations from the Gaussian process

For a Gaussian process with non-zero mean, the definition of the fourth moment of displacement can be expressed as,

$$\mu_4 := \langle \mathbf{r}^2 \rangle^2 + \frac{2}{d} (\langle \mathbf{r}^2 \rangle^2 - \langle \mathbf{r}^4 \rangle). \quad (40)$$

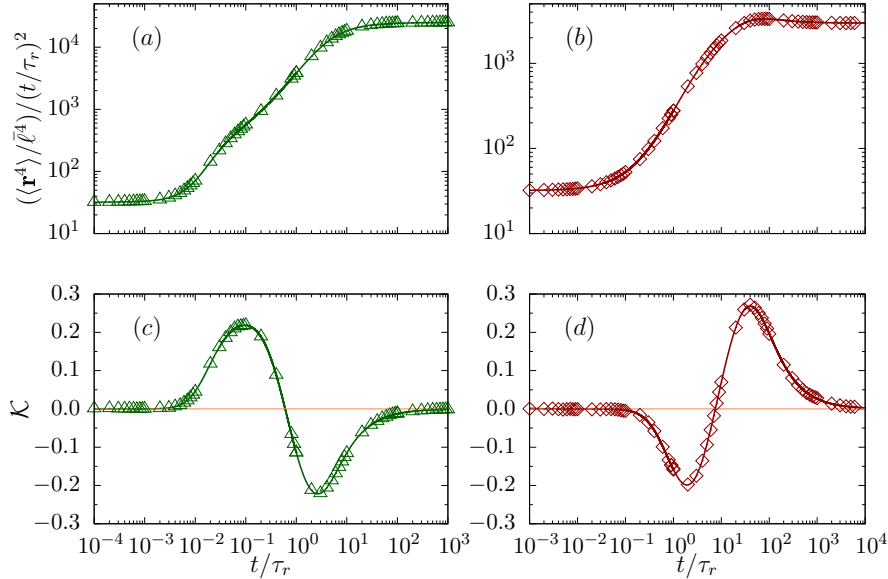


**Figure 6.** (color online) Persistent motion: Plots of  $\langle \mathbf{r}^4 \rangle$  (*a, b*) and Kurtosis ( $\mathcal{K}$ ) (*c, d*) as a function of time in two dimensions. (*a, c*) Parameter values used are  $\tilde{\gamma}_v = 10^2$ ,  $\tilde{D}_v = 4 \times 10^4$ , and  $Pe = 7.07$ . (*b, d*) Parameter values used are  $\tilde{\gamma}_v = 5 \times 10^{-2}$ ,  $\tilde{D}_v = 0.25$ , and  $Pe = 3.54$ . The points denote simulation results averaged over  $10^6$  independent trajectories. The solid lines depict analytic results obtained from the inverse Laplace transform of equation (38). The orange line in (*c, d*) corresponds to zero kurtosis. Initial conditions used are speed  $v_1/\bar{v} = Pe$  and heading direction  $\hat{\mathbf{u}}_0 = \hat{x}$ .

Thus, deviations from such a Gaussian process is captured by the kurtosis

$$\mathcal{K} = \frac{\langle \mathbf{r}^4 \rangle}{\mu_4} - 1. \quad (41)$$

Figure 6(*c, d*) shows the kurtosis as a function of time. A non-zero value of the kurtosis indicates deviations of the stochastic process from a possible Gaussian nature. A positive value appears for distributions with tails longer than normal distributions, while a negative value indicates a tail less extreme than the normal distributions. Figure 6(*c*) corresponds to  $\langle \mathbf{r}^4 \rangle$  in figure 6(*a*) in the limit of  $D_r \gg \gamma_v$ . It shows deviations to positive values at shorter times and negative values at longer times before returning to the Gaussian behavior for long enough trajectories. The plot of kurtosis in figure 6(*d*) corresponds to  $\langle \mathbf{r}^4 \rangle$  in figure 6(*b*) in the limit of  $D_r \ll \gamma_v$ . In contrast to figure 6(*c*), in this parameter regime, the kurtosis shows deviations to negative values at shorter times that changes to positive values at longer times before returning to the Gaussian nature at the longest time scales. As it has been shown in Ref. [21], the orientational fluctuations of the heading direction leads to negative kurtosis in the intermediate times. The positive kurtosis observed here is determined by the active speed fluctuations that was not considered before. In figure 6(*c*) with  $\tilde{\gamma}_v \gg 1$ , the orientational fluctuation time scale is longer than the speed fluctuation time scale. As a result, the negative kurtosis appears at a later time and the positive kurtosis at a shorter time. On the other hand,

in figure 6(d) with  $\tilde{\gamma}_v \ll 1$ , the shorter orientational fluctuation time scale leads to the appearance of negative kurtosis at shorter times and positive kurtosis at longer times. The presence of positive and negative kurtosis in the intermediate times due to the competition between orientational and speed relaxation is the third main result of this paper.

## 8. Discussion

In this paper we presented a detailed study of the dynamics of active Brownian particles with speed fluctuations, in the presence of thermal diffusion. In our model, two independent time scales describe the stochastic change of heading direction and speed. Here we considered the active speed generation using the Schienbein-Gruler model of simple energy pump [36, 37]. We have extended the Fokker-Planck equation based method developed in Ref. [50, 21] to calculate all the relevant dynamical moments of motion in arbitrary dimensions. We presented some of these calculations in detail.

First, we calculated the mean-squared displacement in  $d$ -dimensions starting from the Fokker-Planck approach. The result we derived is consistent with the generic two-time auto-correlation function of active speed. In the limit of a fast relaxation, where the steady-state expression for the speed autocorrelation function can be used, our result for mean-squared displacement reduces to the earlier result obtained for 2d [37, 49]. Moreover, we calculated the fluctuations of the displacement vector, its components along and perpendicular to the initial heading direction, and its fourth moment. These calculations showed several dynamical crossovers that we analyzed in detail and obtained expressions for the crossover times. The number of crossovers observed depends on the parameter values used. Finally, we calculated the kurtosis of the displacement vector to show deviations from the Gaussian process in intermediate times. The kurtosis deviates towards a positive value when the speed fluctuation dominates over the orientation fluctuation and a negative value when the orientation fluctuation dominates over the speed fluctuation. Thus, the kurtosis showed opposite behaviors in the two limits of  $\gamma_v \tau_r \ll 1$  and  $\gamma_v \tau_r \gg 1$ . Our predictions can be tested in experiments on artificial active particles, e.g., self-propulsion of Janus colloids [3, 39, 40]. Our results can be useful in analyzing the dynamics of motile cells having speed and directional fluctuations [42, 43, 44].

## Acknowledgments

The numerical calculations were supported in part by SAMKHYA, the high performance computing facility at Institute of Physics, Bhubaneswar. We thank Abhishek Dhar for useful discussions. D.C. thanks SERB, India for financial support through grant number MTR/2019/000750 and International Centre for Theoretical Sciences (ICTS) for an associateship.

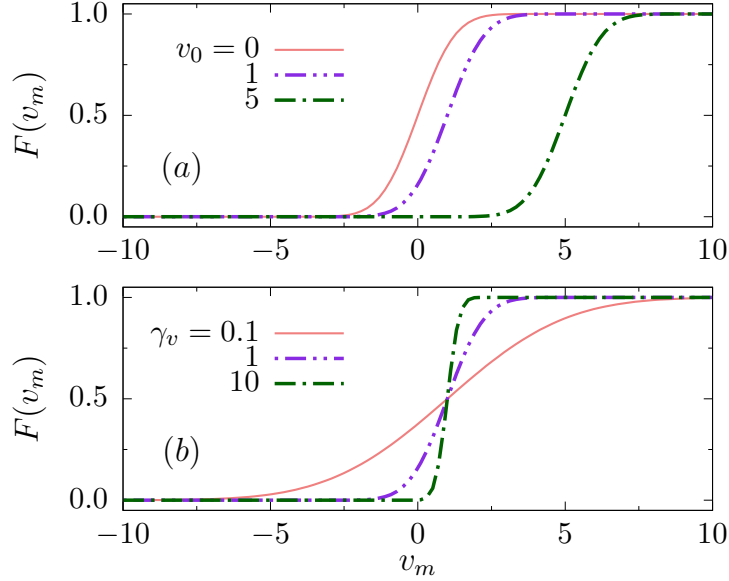


**Figure A1.** (color online) Cumulative distribution function  $F(v_m)$  in equation (A.3) as a function of  $v_m$  at  $\tilde{D}_v = 1$ . (a)  $Pe = 0, 1, 5$  and  $\tilde{\gamma}_v = 1$ . (b)  $\tilde{\gamma}_v = 0.1, 1, 10$  and  $Pe = 1$ .

## Appendix A.

### Steady state probability distribution of speed and its cumulative distribution

The evolution equation of probability distribution of speed  $P(v, t)$  derived from the Schienbein-Gruler mechanism [37] of active speed generation as in equation (2), obeys the following Fokker-Planck equation

$$\partial_t P(v, t) = D_v \partial_v^2 P + \gamma_v \partial_v [(v - v_0)P]. \quad (\text{A.1})$$

The normalized steady-state distribution calculated from equation (A.1) has a Gaussian form peaked around the speed  $v_0$ ,

$$P_s(v) = \left( \frac{\gamma_v}{2\pi D_v} \right)^{1/2} \exp \left( -\frac{\gamma_v}{2D_v} (v - v_0)^2 \right) \quad (\text{A.2})$$

The cumulative distribution function of speed up to a maximum value  $v_m$  is

$$\begin{aligned} F(v_m) &= \left( \frac{\gamma_v}{2\pi D_v} \right)^{1/2} \int_{-\infty}^{v_m} dv \exp \left( -\frac{\gamma_v}{2D_v} (v - v_0)^2 \right) \\ &= \frac{1}{2} \left[ 1 + \operatorname{erf} \left( \frac{v_m - v_0}{\sqrt{2D_v/\gamma_v}} \right) \right]. \end{aligned} \quad (\text{A.3})$$

In figure A1, we show the variation of cumulative distribution function for speed with changing  $Pe = v_0/\bar{v}$  and  $\tilde{\gamma}_v = \gamma_v \tau_r$ . The probability of getting negative speed, an effective active speed opposite to the heading direction, decreases with increase of  $v_0$  and  $\gamma_v$ .

## Appendix B.

### Autocorrelation of active speed

Here, we calculate the active speed auto-correlation function directly from the governing Langeving equation (2). The formal solution of equation (2) with the initial condition  $v(t=0) = v_1$  is

$$v(t) = v_1 e^{-\gamma_v t} + \int_0^t \left( \gamma_v v_0 + \sqrt{2D_v} \Lambda(t') \right) e^{-\gamma_v(t-t')} dt', \quad (\text{B.1})$$

with  $\langle \Lambda(t) \rangle = 0$ , and  $\langle \Lambda(t) \Lambda(t') \rangle = \delta(t-t')$ . In this expression, the integration of the second term gives,

$$I = \int_0^t \gamma_v v_0 e^{-\gamma_v(t-t')} dt' = \gamma_v v_0 e^{-\gamma_v t} \int_0^t e^{\gamma_v t'} dt' = v_0 (1 - e^{-\gamma_v t}).$$

This allows us to calculate the instantaneous mean speed

$$\langle v(t) \rangle = v_1 e^{-\gamma_v t} + v_0 (1 - e^{-\gamma_v t}). \quad (\text{B.2})$$

Thus, the deviation of speed from its mean value

$$\delta v(t) \equiv v(t) - \langle v(t) \rangle = \sqrt{2D_v} e^{-\gamma_v t} \int_0^t \Lambda(t') e^{\gamma_v t'} dt'. \quad (\text{B.3})$$

As a result, the speed autocorrelation function of speed fluctuations can be calculated as

$$\langle \delta v(t_1) \delta v(t_2) \rangle = 2D_v e^{-\gamma_v(t_1+t_2)} \int_0^{t_1} dt'_1 \int_0^{t_2} dt'_2 e^{\gamma_v(t'_1+t'_2)} \delta(t'_1 - t'_2) \quad (\text{B.4})$$

If  $(t_1 > t_2)$ , the  $\delta(t'_1 - t'_2)$  restricts the integration over  $t'_1 = t'_2$  line, then  $t'_1$  effectively runs up to  $t_2$ .

$$\langle \delta v(t_1) \delta v(t_2) \rangle = \frac{D_v}{\gamma_v} [e^{-\gamma_v(t_1-t_2)} - e^{-\gamma_v(t_1+t_2)}] \quad (\text{B.5})$$

The steady state correlation may be obtained by, letting  $t_1, t_2 \rightarrow \infty$  and keeping  $\tau = t_1 - t_2$  finite,

$$\langle \delta v(\tau) \delta v(0) \rangle = \frac{D_v}{\gamma_v} e^{-\gamma_v \tau}. \quad (\text{B.6})$$

In the steady state limit the instantaneous fluctuation,  $\langle \delta v^2(0) \rangle = D_v / \gamma_v$ . Thus we may write, speed correlation in normalized form,

$$\frac{\langle \delta v(\tau) \delta v(0) \rangle}{\langle \delta v^2(0) \rangle} = e^{-\gamma_v \tau} \quad (\text{B.7})$$

The fluctuation in speed can be derived from equation (B.5) by setting  $t_1 = t_2 \equiv t$ ,

$$\frac{\langle \delta v^2(t) \rangle}{\langle \delta v^2(0) \rangle} = (1 - e^{-2\gamma_v t}). \quad (\text{B.8})$$

## References

- [1] Frank Schweitzer. *Brownian Agents and Active Particles*. Springer, Heidelberg, 2003.
- [2] M. C. Marchetti, J. F. Joanny, S. Ramaswamy, T. B. Liverpool, J. Prost, Madan Rao, and R. Aditi Simha. Hydrodynamics of soft active matter. *Rev. Mod. Phys.*, 85(3):1143–1189, jul 2013.
- [3] Clemens Bechinger, Roberto Di Leonardo, Hartmut Löwen, Charles Reichhardt, Giorgio Volpe, and Giovanni Volpe. Active Particles in Complex and Crowded Environments. *Rev. Mod. Phys.*, 88(4):045006, nov 2016.
- [4] P Romanczuk, M Bär, W Ebeling, B. Lindner, and L. Schimansky-Geier. Active Brownian particles. *Eur. Phys. J. Spec. Top.*, 202:1–162, 2012.
- [5] Gerhard Gompper, Roland G. Winkler, Thomas Speck, Alexandre Solon, Cesare Nardini, Fernando Peruani, Hartmut Löwen, Ramin Golestanian, U. Benjamin Kaupp, Luis Alvarez, Thomas Ki rboe, Eric Lauga, Wilson C.K. Poon, Antonio Desimone, Santiago Mui&ntilde;os-Landin, Alexander Fischer, Nicola A. Söker, Frank Cichos, Raymond Kapral, Pierre Gaspard, Marisol Ripoll, Francesc Sagues, Amin Doostmohammadi, Julia M. Yeomans, Igor S. Aranson, Clemens Bechinger, Holger Stark, Charlotte K. Hemelrijk, Fran ois J. Nedelec, Trinish Sarkar, Thibault Aryaksama, Mathilde Lacroix, Guillaume Duclos, Victor Yashunsky, Pascal Silberzan, Marino Arroyo, and Sohan Kale. The 2020 motile active matter roadmap. *J. Phys. Condens. Matter*, 32(19), 2020.
- [6] R. Dean Astumian and Peter Hänggi. Brownian motors. *Physics Today*, 55(11):33–39, jan 2002.
- [7] Peter Reimann. Brownian motors: Noisy transport far from equilibrium. *Physics Report*, 361(2-4):57–265, apr 2002.
- [8] Howard C. Berg and Douglas A. Brown. Chemotaxis in *Escherichia coli* analysed by three-dimensional tracking. *Nature*, 239(5374):500–504, 1972.
- [9] C. A. Condat, J. Jäckle, and S. A. Menchón. Randomly curved runs interrupted by tumbling: A model for bacterial motion. *Physical Review E*, 72(2), 2005.
- [10] Hiro Sato Niwa. Self-organizing dynamic model of fish schooling. *Journal of Theoretical Biology*, 171(2):123–136, nov 1994.
- [11] M E Cates and J Tailleur. When are active Brownian particles and run-and-tumble particles equivalent? Consequences for motility-induced phase separation. *EPL (Europhysics Lett.)*, 101(2):20010, jan 2013.
- [12] Étienne Fodor, Cesare Nardini, Michael E. Cates, Julien Tailleur, Paolo Visco, and Frédéric van Wijland. How Far from Equilibrium Is Active Matter? *Phys. Rev. Lett.*, 117(3):038103, jul 2016.
- [13] Shibnanda Das, Gerhard Gompper, and Roland G. Winkler. Confined active Brownian particles: theoretical description of propulsion-induced accumulation. *New J. Phys.*, 20(1):015001, jan 2018.
- [14] Francisco J Sevilla and Luis A Gomez Nava. Theory of diffusion of active particles that move at constant speed in two dimensions. *Physical Review E*, 90(2):022130, 2014.
- [15] R. Großmann, F. Peruani, and M. Bär. Diffusion properties of active particles with directional reversal. *New J. Phys.*, 18(4), 2016.
- [16] Christina Kurzthaler, Clémence Devailly, Jochen Arlt, Thomas Franosch, Wilson C.K. Poon, Vincent A. Martinez, and Aidan T. Brown. Probing the Spatiotemporal Dynamics of Catalytic Janus Particles with Single-Particle Tracking and Differential Dynamic Microscopy. *Phys. Rev. Lett.*, 121(7):078001, aug 2018.
- [17] Urna Basu, Satya N. Majumdar, Alberto Rosso, and Grégory Schehr. Active Brownian motion in two dimensions. *Phys. Rev. E*, 98(6):062121, 2018.
- [18] Kanaya Malakar, V. Jemseena, Anupam Kundu, K. Vijay Kumar, Sanjib Sabhapandit, Satya N. Majumdar, S. Redner, and Abhishek Dhar. Steady state, relaxation and first-passage properties of a run-and-tumble particle in one-dimension. *J. Stat. Mech. Theory Exp.*, 2018(4):043215, apr 2018.

- [19] Urna Basu, Satya N. Majumdar, Alberto Rosso, and Grégory Schehr. Long-time position distribution of an active Brownian particle in two dimensions. *Phys. Rev. E*, 100(6):062116, dec 2019.
- [20] Abhishek Dhar, Anupam Kundu, Satya N. Majumdar, Sanjib Sabhapandit, and Grégory Schehr. Run-and-tumble particle in one-dimensional confining potentials: Steady-state, relaxation, and first-passage properties. *Phys. Rev. E*, 99(3):032132, mar 2019.
- [21] Amir Shee, Abhishek Dhar, and Debasish Chaudhuri. Active Brownian particles: mapping to equilibrium polymers and exact computation of moments. *Soft Matter*, 16(20):4776–4787, 2020.
- [22] Ion Santra, Urna Basu, and Sanjib Sabhapandit. Run-and-tumble particles in two dimensions: Marginal position distributions. *Phys. Rev. E*, 101(6):062120, jun 2020.
- [23] Satya N. Majumdar and Baruch Meerson. Toward the full short-time statistics of an active brownian particle on the plane. *Phys. Rev. E*, 102:022113, Aug 2020.
- [24] Kanaya Malakar, Arghya Das, Anupam Kundu, K. Vijay Kumar, and Abhishek Dhar. Steady state of an active Brownian particle in a two-dimensional harmonic trap. *Phys. Rev. E*, 101(2):022610, feb 2020.
- [25] Urna Basu, Satya N. Majumdar, Alberto Rosso, Sanjib Sabhapandit, and Grégory Schehr. Exact stationary state of a run-and-tumble particle with three internal states in a harmonic trap. *J. Phys. A Math. Theor.*, 53(9), 2020.
- [26] Ion Santra, Urna Basu, and Sanjib Sabhapandit. Run-and-tumble particles in two dimensions: Marginal position distributions. *Phys. Rev. E*, 101:062120, Jun 2020.
- [27] Ion Santra, Urna Basu, and Sanjib Sabhapandit. Active Brownian motion with directional reversals. *Phys. Rev. E*, 104(1), 2021.
- [28] Debasish Chaudhuri and Abhishek Dhar. Active Brownian particle in harmonic trap: exact computation of moments, and re-entrant transition. *Journal of Statistical Mechanics: Theory and Experiment*, 2021(1):013207, jan 2021.
- [29] Francesco Mori, Pierre Le Doussal, Satya N. Majumdar, and Grégory Schehr. Condensation transition in the late-time position of a run-and-tumble particle. *Phys. Rev. E*, 103:062134, Jun 2021.
- [30] David S. Dean, Satya N. Majumdar, and Hendrik Schawe. Position distribution in a generalized run-and-tumble process. *Phys. Rev. E*, 103:012130, Jan 2021.
- [31] Gabriel S. Redner, Michael F. Hagan, and Aparna Baskaran. Structure and Dynamics of a Phase-Separating Active Colloidal Fluid. *Phys. Rev. Lett.*, 110(5):055701, jan 2013.
- [32] Yaouen Fily, Aparna Baskaran, and Michael F Hagan. Dynamics of self-propelled particles under strong confinement. *Soft Matter*, 10:5609–17, 2014.
- [33] Rolf E. Isele-Holder, Jens Elgeti, and Gerhard Gompper. Self-propelled worm-like filaments: spontaneous spiral formation, structure, and dynamics. *Soft Matter*, 11(36):7181–7190, 2015.
- [34] Roland G. Winkler and Gerhard Gompper. The physics of active polymers and filaments. *J. Chem. Phys.*, 153(4):040901, jul 2020.
- [35] Nisha Gupta, Abhishek Chaudhuri, and Debasish Chaudhuri. Morphological and dynamical properties of semiflexible filaments driven by molecular motors. *Phys. Rev. E*, 99(4):042405, apr 2019.
- [36] M. Schienbein and H. Gruler. Langevin equation, Fokker-Planck equation and cell migration. *Bulletin of Mathematical Biology*, 55(3):585–608, may 1993.
- [37] M. Schienbein, K. Franke, and H. Gruler. Random walk and directed movement: Comparison between inert particles and self-organized molecular machines. *Physical Review E*, 49(6):5462–5471, jun 1994.
- [38] Frank Schweitzer, Werner Ebeling, and Benno Tilch. Complex motion of Brownian particles with energy depots. *Phys. Rev. Lett.*, 80(23):5044–5047, 1998.
- [39] Jonathan R Howse, Richard AL Jones, Anthony J Ryan, Tim Gough, Reza Vafabakhsh, and Ramin Golestanian. Self-motile colloidal particles: from directed propulsion to random walk. *Physical review letters*, 99(4):048102, 2007.

- [40] Hong Ren Jiang, Natsuhiko Yoshinaga, and Masaki Sano. Active motion of a Janus particle by self-thermophoresis in a defocused laser beam. *Phys. Rev. Lett.*, 105(26):1–4, 2010.
- [41] Patrick Pietzonka and Udo Seifert. Entropy production of active particles and for particles in active baths. *J. Phys. A Math. Theor.*, 51(1):01LT01, jan 2018.
- [42] David Selmecki, Stephan Mosler, Peter H. Hagedorn, Niels B. Larsen, and Henrik Flyvbjerg. Cell Motility as Persistent Random Motion: Theories from Experiments. *Biophys. J.*, 89(2):912–931, aug 2005.
- [43] Giacomo Frangipane, Gaszton Vizsnyiczai, Claudio Maggi, Romolo Savo, Alfredo Sciortino, Sylvain Gigan, and Roberto Di Leonardo. Invariance properties of bacterial random walks in complex structures. *Nat. Commun.*, 10(1):2442, dec 2019.
- [44] Stefan Otte, Emiliano Perez Ipiña, Rodolphe Pontier-Bres, Dorota Czerucka, and Fernando Peruani. Statistics of pathogenic bacteria in the search of host cells. *Nat. Commun.*, 12(1):1990, dec 2021.
- [45] Benjamin De Bruyne, Satya N. Majumdar, and Grégory Schehr. Survival probability of a run-and-tumble particle in the presence of a drift. *J. Stat. Mech. Theory Exp.*, 2021(4), 2021.
- [46] Francesco Mori, Pierre Le Doussal, Satya N. Majumdar, and Grégory Schehr. Universal properties of a run-and-tumble particle in arbitrary dimension. *Phys. Rev. E*, 102:042133, Oct 2020.
- [47] Francesco Mori, Pierre Le Doussal, Satya N. Majumdar, and Grégory Schehr. Universal survival probability for a  $d$ -dimensional run-and-tumble particle. *Phys. Rev. Lett.*, 124:090603, Mar 2020.
- [48] Giacomo Gradenigo and Satya N. Majumdar. A first-order dynamical transition in the displacement distribution of a driven run-and-tumble particle. *J. Stat. Mech. Theory Exp.*, 2019(5), 2019.
- [49] Fernando Peruani and Luis G. Morelli. Self-Propelled Particles with Fluctuating Speed and Direction of Motion in Two Dimensions. *Phys. Rev. Lett.*, 99(1):010602, jul 2007.
- [50] J. J. Hermans and R. Ullman. The statistics of stiff chains, with applications to light scattering. *Physica*, 18(11):951–971, 1952.
- [51] Kiyosi Itô. *International Symposium on Mathematical Problems in Theoretical Physics*, chapter Stochastic Calculus, pages 218–223. Springer-Verlag, Berlin-Heidelberg-New York, 1975.
- [52] M. van den Berg and J. T. Lewis. Brownian Motion on a Hypersurface. *Bulletin of the London Mathematical Society*, 17(2):144–150, mar 1985.
- [53] Aleksandar Mijatović, Veno Mramor, and Gerónimo Uribe Bravo. A note on the exact simulation of spherical brownian motion. *Statistics & Probability Letters*, page 108836, 2020.